Neurobiology of Disease 129 (2019) 217–233

Contents lists available at ScienceDirect

Neurobiology of Disease

journal homepage: www.elsevier.com/locate/ynbdi

New piperazine multi-effect drugs prevent neurofibrillary degeneration and amyloid deposition, and preserve memory in animal models of Alzheimer's disease

Nicolas Sergeant[a,**], Valérie Vingtdeux[a,1], Sabiha Eddarkaoui[a,1], Marion Gay[a], Caroline Evrard[a], Nicolas Le Fur[a], Cyril Laurent[a], Raphaelle Caillierez[a], Hélène Obriot[a], Paul-Emmanuel Larchanché[a], Amaury Farce[b], Mathilde Coevoet[a], Pascal Carato[a,2], Mostafa Kouach[c], Amandine Descat[c], Patrick Dallemagne[d], Valérie Buée-Scherrer[a], David Blum[a], Malika Hamdane[a], Luc Buée[a], Patricia Melnyk[a,*]

[a] Univ. Lille, Inserm, CHU Lille, UMR-S1172 – JPArc – Centre de Recherche Jean-Pierre Aubert Neurosciences et Cancer, F-59000 Lille, France
[b] Univ. Lille, Inserm, CHU Lille, U995 – LIRIC – Lille Inflammation Research International Center, F-59000 Lille, France
[c] Univ. Lille, CUMA – Centre Universitaire de Mesures et d'Analyses, F-59000 Lille, France
[d] UNICAEN, UFR des Sciences Pharmaceutiques, EA 4258 CERMN, F-14032 Caen, France

ARTICLE INFO

Keywords:
Alzheimer's disease
Amyloid
Microtubule-associated protein tau
Multi-effect drugs
Neurofibrillary tangles
Tauopathies
Acetylcholinesterase

ABSTRACT

Alzheimer's Disease is a devastating dementing disease involving amyloid deposits, neurofibrillary tangles, progressive and irreversible cognitive impairment. Today, only symptomatic drugs are available and therapeutic treatments, possibly acting at a multiscale level, are thus urgently needed. To that purpose, we designed multi-effects compounds by synthesizing drug candidates derived by substituting a novel *N,N′*-disubstituted piperazine anti-amyloid scaffold and adding acetylcholinesterase inhibition property. Two compounds were synthesized and evaluated. The most promising hybrid molecule reduces both the amyloid pathology and the Tau pathology as well as the memory impairments in a preclinical model of Alzheimer's disease. *In vitro* also, the compound reduces the phosphorylation of Tau and inhibits the release of Aβ peptides while preserving the processing of other metabolites of the amyloid precursor protein.

We synthetized and tested the first drug capable of ameliorating both the amyloid and Tau pathology in animal models of AD as well as preventing the major brain lesions and associated memory impairments. This work paves the way for future compound medicines against both Alzheimer's-related brain lesions development and the associated cognitive impairments.

1. Introduction

Alzheimer's disease (AD) is a disease that entails neurodegeneration and dementia and has no cure yet. AD associates two principal neuropathological components, namely extracellular amyloid deposits and neurofibrillary tangles (NFTs). The amyloid pathology is characterized by abnormal production of pro-aggregative and synaptotoxic amyloid-β (Aβ) species that are the building blocks of extracellular amyloid deposits. NFTs result from the abnormal phosphorylation of isoforms of the microtubule-associated protein Tau and their progressive

Abbreviations: AChE, acetylcholinesterase; AD, Alzheimer's Disease; ADME, Absorption Distribution Metabolism Excretion; AICD, APP Intra Cellular Domain; APP, amyloid precursor protein; BACE 1, Beta-site Amyloid-precursor-protein-Cleaving Enzyme 1; Baf, Bafilomycin; BBB, Blood Brain Barrier; CQ, Chloroquine; CTF, carboxy-terminal fragment; NFT, neurofibrillary tangles; NICD, Notch Intra Cellular Domain; PS1, Pre-Senilin 1

* Correspondence to: Patricia Melnyk, Inserm UMR-S1172 - Team Onco and Neurochemistry, School of Pharmacy, 3 rue du Pr. Laguesse, BP 83, 59006 Lille cedex, France.

** Correspondence to: Nicolas Sergeant, Inserm UMR-S1172 - Team Alzheimer & Tauopathies - Bât. Biserte, Univ. de Lille - rue M. Polonowski, 59045 Lille cedex, France.

E-mail addresses: nicolas.sergeant@inserm.fr (N. Sergeant), patricia.melnyk@univ-lille.fr (P. Melnyk).

[1] Equal contribution.

[2] Present address: Univ Poitiers, CNRS IC2MP UMR 7285, F-86073 Poitiers, France.

https://doi.org/10.1016/j.nbd.2019.03.028
Received 24 July 2018; Received in revised form 1 March 2019; Accepted 26 March 2019
Available online 27 March 2019
0969-9961/

accumulation and aggregation into fibrils in neurons (Dubois et al., 2010). NFTs are known to affect the cholinergic system in AD and their spatiotemporal distribution is tightly correlated with cognitive impairments. Moreover, the progression of 'Tau pathology' is also correlated with increased concentrations of brain Aβ peptides and the loss of APP metabolites (Sergeant et al., 1999). A growing body of evidence supports the notion that these two pathological processes are both causatives of the disease and might even have a synergistic effect on the progression of the symptoms (Sergeant et al., 2002; Ittner et al., 2010; Takahashi et al., 2015; Pooler et al., 2015). Thereby, a promising therapeutic approach could be to tackle the causes and effects of both amyloid and Tau pathologies (Mangialasche et al., 2010). Nevertheless, disease-modifying small molecules currently in clinical trials only act on either one or the other of these processes or are supposed to cure the symptoms (Cummings et al., 2017). A multi-target directed ligands strategy has already been suggested for multifactorial diseases (Capurro et al., 2013).

We previously described *N,N′*-disubstituted piperazine scaffold (Melnyk et al., 2006; Melnyk et al., 2015) which are able to reduce the release of Aβ species and increase the amount of APP metabolites. These compounds targeted both amyloid and tau pathologies as well as the cognitive functions in well-characterized mouse models of either amyloid or Tau pathology (Barrier et al., 2012). The lead compound of this family, **AZP2006**, is in clinical phase 1. On the other hand, acetylcholinesterase inhibitors are anti-Alzheimer's drugs available in the market. We describe herein multi-effect molecules that combine an *N,N′*-disubstituted piperazine scaffold and acetylcholinesterase (AChE) inhibitors in a single molecule. Thus, as proof-of-concept, two multi-effect molecules were synthesized, starting from AchE inhibitors Tacrine and Rivastigmine. Notably, one of the compounds substituted with Tacrine (**RPEL**) not only preserved AD mice from cognitive deterioration and reduced the amyloid pathology but also significantly reduced the Tau pathology. No adverse effect related to cholinergic toxicity could be registered. This work validates the challenging strategy for the design of multi-effect drugs as a substantial breakthrough and identifies **RPEL** as a lead compound for the development of a multi-faceted treatment for AD.

2. Material and methods

2.1. Synthesis of compounds

Both mixed compounds **RPEL** and **MAG** were obtained from a common intermediate **1**, synthesized from commercially available 3-[4-(3-aminopropyl)piperazin-1-yl]propan-1-amine (Scheme 1). The synthetic pathway is characterized by protection, deprotection reactions, Palladium cross couplings and reductive aminations ((Hu (2001), Ryckebusch et al. (2003)). This pathway allows also the synthesis of **RPEL-d$_{14}$**, used as the internal standard in quantitative dosage.

2.2. AChE inhibition

The inhibitory capacity of compounds on AChE biological activity was evaluated using the spectrometric method of Ellman (Ellman et al., 1961). Acetylthiocholine iodide and 5,5-dithiobis-(2-nitrobenzoic) acid (DTNB) were purchased from Sigma Aldrich. AChE from human erythrocytes (buffered aqueous solution, ≥500 units/mg protein (BCA), Sigma Aldrich) was diluted in 20 mM HEPES buffer pH 8, with 0.1% Triton X-100 such as to obtain an enzyme solution with 0.25 unit/mL enzyme activity. In a 96-well plate, 100 µL of 0.3 mM DTNB dissolved in phosphate buffer pH 7.4 was added followed by 50 µL of test compound solution and 50 µL of enzyme (0.05 U final). After 5 min of pre-incubation at 25 °C, the reaction was initiated by the injection of 50 µL of 10 mM acetylthiocholine iodide solution. The hydrolysis of acetylthiocholine was monitored by the formation of yellow 5-thio-2-nitrobenzoate anion as the result of the reaction of DTNB with thiocholine, released by the enzymatic hydrolysis of acetylthiocholine, at a wavelength of 412 nm, using a 96-well microplate reader (TECAN Infinite M200, Lyon, France). Test compounds were dissolved in analytical grade DMSO. The rate of increase of absorbance at 412 nm was followed every minute for 10 min. Assays were performed with a blank containing all components except acetylthiocholine, in order to account for non-enzymatic reactions. The reaction slopes were compared and the percent inhibition due to the presence of test compounds was calculated by the following expression: 100 - (v_i/v_0x100) where v_i is the rate calculated in the presence of inhibitor and v_0 is enzyme activity. IC_{50} values were determined graphically by plotting the percentage of inhibition versus the logarithm of six inhibitor concentrations in the assay solution, using Origin software.

2.3. Antibodies

The primary antibodies used herein included: a rabbit antiserum against the last 17 amino acids of APP, named APP-C17 (Sergeant et al., 2002; Vingtdeux et al., 2007). The Myc-Tag (9B11) monoclonal antibody (Cell Signaling) was used to study ΔE Notch processing (Vingtdeux et al., 2007). The WO-2 (Millipore) or 6E8 (Covance) antibodies were directed against the N-terminal region of the human Aβ peptide. The APP-8E5 antibody was kindly provided by Peter Seubert (Elan Pharmaceutical) and recognizes the APP sequence 444–592 (numbering according to the APP695 isoform). The BACE1 antibody was a rabbit purified polyclonal antibody raised against a synthetic peptide of the human BACE1 sequence 458–501 (Millipore). Pan-Tau and phospho-dependent Tau antibodies included Tau-Nter (M19G, 1/10000, Tau-Cter (1/10000) (Sergeant et al., 2007), Tau-1 (1/5000, Merck Millipore), S199P (directed against phosphoserine 199, 1/4000, Sergeant et al. (2007), from SPQI-4BioDx, France), Tau-Phospho 396 (1/10000, Life Technologies), Tau-Phospho 404 (1/10000, Life Technologies), 422 (clone 2H9, a monoclonal antibody developed against a phospho-peptide containing the phosphorylated serine 422 residue of Tau, numbering according to the longest human brain tau-441 isoform, from SPQI-4BioDx, France), AT8 (1/1000) and AT270 (1/2000), AT100 (1/1000) were purchased from Thermo Scientific. Neuron-specific enolase (1/10000), β-actin (1/5000) and β-tubulin (1/10000) were from Sigma-Aldrich.

2.4. Cell culture and transfection

The human neuroblastoma cell line SKNSH-SY5Y (SY5Y) was maintained in Dulbecco's modified Eagle medium (DMEM) supplemented with 10% fetal calf serum, 2 mM L-glutamine, 1 mM non-essential amino acids, penicillin/streptomycin (Life Sciences Technology) in a 5% CO_2 humidified incubator at 37 °C. Human APP695 cDNA was sub-cloned into the eukaryotic expression vector pcDNA3.1 (Invitrogen), allowing for antibiotic selection with G418. This plasmid was transfected into SY5Y cells using the ethyleneimine polymer ExGen 500 (Euromedex) according to the manufacturer's instructions. SY5Y-expressing the WT APP695 isoforms were selected by the addition of 200 µg/mL G418 to the cell culture medium and one clone, named SY5Y-APP^{695WT}, was used. For the transient expression of ΔE Notch (Notch I lacking the extracellular domain), SY5Y cells were transfected with Myc-tagged ΔE Notch (kindly provided by Pr. Raphael Kopan; Washington University, St. Louis, MO, USA) using the FuGENE® HD transfection reagent according to the manufacturer's instructions (Roche). Cells were collected 24 h after drug treatment. The inducible SY5Y-Tau46 (corresponding to the human brain isoform of 412 amino acids, including coding sequences for exon 2 and 10) has been described previously (Bretteville et al., 1999). Briefly, to induce human Tau 412 protein expression, SY5Y-Tau46 cells were treated for 24 h with 1 µg/mL of tetracycline and induced SY5Y-Tau46 cells were further treated for 24 h with drugs at the indicated concentrations. Protein lysates were obtained as indicated under drug treatment. Cell culture

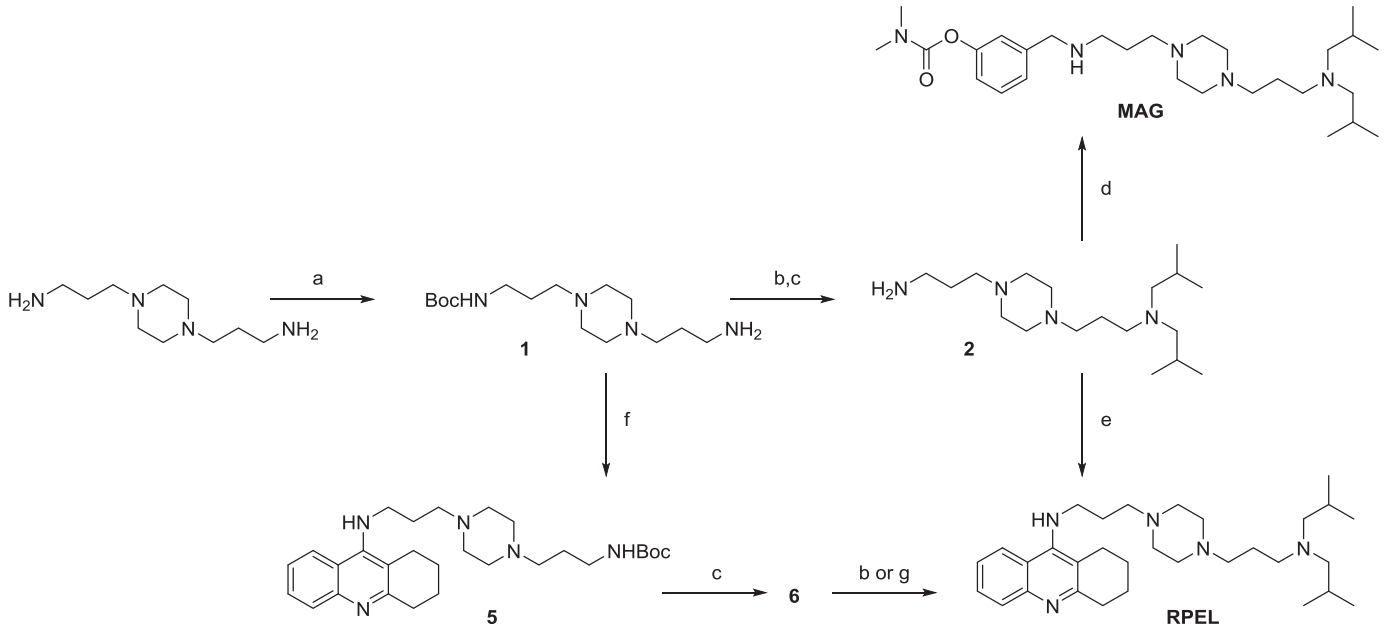

Scheme 1. Synthesis of MAG and RPEL compounds.
Reagents and conditions: (a) Boc_2O (0.3 eq), DCM, 20 °C, 2 days, 99%; (b) isobutyraldehyde (4.1 eq), TEA (1.2 eq), $NaBH_4$ (6.0 eq), MeOH, 20 °C, 24 h, 50–58%; (c) dioxane saturated with HCl_g, 20 °C, 12 h, 99%; (d) 3-formylphenyl-*N*,*N*-dimethylcarbamate **3** (1.1 eq), $NaBH_4$ (6.5 eq), MeOH, 20 °C, 2 days, 76%; (e) (+/−) BINAP (0.15 eq), Cs_2CO_3 (0.8 eq), Pd_2dba_3 (0.3 eq), dioxane, reflux, 12 h, 75%; (f) 9-chloro-1,2,3,4-tetrahydroacridine **2** (1.2 eq), Cs_2CO_3 (1.4 eq), Xantphos (0.15 eq), Pd_2dba_3 (0.05 eq), dioxane, reflux, 1 day, 90%; (g) isobutyraldehyde-d_7 (4.0 eq), $NaBH(OAc)_3$ (4.0 eq), DCM, 20 °C, 15 h, 34%.

and treatment conditions were the same as for the SY5Y-APP^{695WT} cell-line.

2.5. In vitro metabolic stability (mouse liver microsomes)

RPEL stock solutions were diluted in 100 mM potassium phosphate buffer (KPi, 1 μM final concentrations) pH = 7.4, and test compounds were then incubated for 60 min in an incubator-shaker (Eppendorf) at 37 °C and 1400 rpm with regenerating system (NADPH) and microsomal preparation (male mice, BD Biosciences, final concentration 0.3 mg/mL in KPi buffer). Reactions were stopped with cold acetonitrile and Internal Standard (IS) CQ diphosphate was then added for further quantification (based upon Test compound/IS ratio area). Samples were mixed thoroughly and then centrifuged at 13000 rpm for 10 min. Supernatants were evaporated with an under vacuum system (Speedvac) at medium drying rate for 2 h and reconstitution of residues was achieved in water + 0.1% TFA. 10 μL injections were finally performed in the LC/MS system. Microsomal stability was calculated upon area ratio of parent compounds at different times.

The LC/MS system consisted of an Orbitrap Exactive instrument (Thermo) equipped with an electrospray ionization source used in positive mode ($M + H^+$). The apparatus was managed with Xcalibur software. Tune parameters were set as: Sheet gas flow rate at 70 L/min, Aux gas flow rate at 20 L/min, spray voltage at 3.00 kV, capillary temperature at 275 °C, capillary voltage at 95 V, tube lens voltage at 165 V and skimmer voltage at 36 V. Tray temperature was fixed at 4 °C and oven at 30 °C. The analytical column was a C18 Hypersil Gold Thermo 50 × 2 mm, 1.9 μm (Thermo). The mobile phase consisted of water + 0.05% TFA (A) and acetonitrile + 0.05%TFA (B). The linear gradient elution program was as follows: 0–100% of B over 3.5 min, followed by an isocratic hold at 100% B for 1 min and 2 min of re-equilibration with 100% A for a total run of 6 min at a flow rate of 400 μL/min. Due to the basicity of polyamines, good sensitivity was achieved using TFA in the mobile phase.

2.6. Drug treatment

For the drug treatment, SY5Y-APP^{695WT} cells were maintained in 75 cm^2 culture flasks (Falcon) until they reached 80% confluency. The cells were recovered with Trypsin-EDTA, split and plated on 12-well plates (Falcon), 24 h before drug exposure. Preceding the addition of the drugs, cultures were quickly rinsed once with warm (37 °C) phosphate-buffered saline (PBS) solution and then exposed to drugs at the indicated concentrations for 24 h. Drugs from a 10 mM stock solution in water were diluted at the desired final concentrations in supplemented DMEM without antibiotic. After 24, 48, or 72 h, the conditioned-cell medium was collected in polypropylene tubes (Eppendorf) and directly frozen at −80 °C while awaiting the eventual measurement of its Aβ peptide content. The drugs used were as follows: the lysosomotropic and autophagic flux inhibitor CQ (Sigma-Aldrich), the vacuolar-type H^+ ATPase inhibitor Baf (Merck Millipore), the γ-secretase inhibitors L685 and Compound E (Enzo Life Sciences), the γ-secretase inhibitor XVI/DAPM (Merck Millipore), DAPT (Sigma-Aldrich). Treated SY5Y-APP^{695WT} cells were rinsed once with warm PBS. The PBS was discarded and 100 μL of warm (60 °C) LDS-lysis buffer (Invitrogen) with protease inhibitors (Complete Mini EDTA-Free, Roche Molecular Biochemicals) was added. Cells were scraped with a rubber policeman, the lysate was recovered and rapidly sonicated before heat treatment for 10 min at 100 °C. Protein concentration was determined using the Pierce BCA Protein Assay, Reducing Agent Compatible (RAC) (Thermoscientific) and samples were kept at −80 °C until used.

2.7. Cytotoxicity

Cytotoxicity was measured using 3-(4,5-dimethylthiazol-2-yl)-5-(3-carboxymethoxyphenyl)-2-(4-sulfophenyl)-2H-tetrazolium (MTS) tests. SY5Y-APP^{695WT} cells were plated in 96-wells plate at 3.10^4 cells per well and allowed to attach for 24 h. Cells were then incubated with 100 μL of DMEM medium with 10% SVF containing (or not) the defined concentration of drugs. Cytotoxicity was determined by using the colorimetric MTS assay (CellTiter 96® Aqueous One Solution Cell Proliferation Assay-MTS Promega) according to the manufacturer's

instructions. Absorbance was read at 490 nm.

2.8. In vitro assay for γ-secretase

Three 75 cm^2 flasks of SY5Y-APP^{695WT} cells were rinsed once with PBS at 37 °C before the addition of 1 mL of hypotonic MOPS buffer [10 mM MOPS (Sigma-Aldrich), 10 mM KCl (Merck)]. Cells were scraped with a rubber policeman and lysed using a glass Potter homogenizer. Cell homogenates were spun at 1000 g at 4 °C for 15 min and the protein concentration in post-nuclear supernatant was determined with a BCA protein concentration assay kit (BioRad) according to the manufacturer's instructions. Each condition was carried out in triplicate and the whole assay was repeated independently three times. Post-nuclear supernatant was fractionated in aliquots containing a total of 1 mg of protein and then centrifuged at 16,000 ×g at 4 °C for 40 min. Supernatants were discarded and the pellets were re-suspended in 100 µL of γ-secretase assay buffer [Sodium Citrate 150 mM (Sigma-Aldrich) and Complete mini EDTA-Free Protease inhibitor (Roche)]. Drugs were added as follows: L685 (100 nM), DAPT (200 nM), DAPM (200 nM), CpdE (200 nM), Baf (100 nM), CQ (5 µM) and **RPEL** or **MAG** at 3, 5 and 10 µM. For the control reaction in which the γ-secretase is inhibited, the homogenates were incubated at 4 °C whereas the γ-secretase reaction was carried out at 37 °C for 6 h. Homogenates were placed on ice and 25 µL of 2× SDS-PAGE loading buffer (20 mM Tris-HCl pH 6.8, 20 mM DTT, 5% SDS and 20% glycerol) was added to 50 µL of the homogenates which were boiled for 10 min at 100 °C.

2.9. Primary neuronal cultures and drug treatment

Primary neuron cultures were obtained from the dissection of fetuses' forebrains obtained from C57BL6 wild-type female mice that were sacrificed at 18,5 days of gestation as described previously (Domise et al., 2016). **RPEL** treatments at 5 or 10 µM were realized directly in the culture media for 24 h at div 17.

2.10. Study approval

All *in vivo* protocols were approved by the local ethics committee (n°342,012, CEEA).

2.11. Animals treatment

3 month-old WT C57Bl/6 J mice were purchased from Charles Rivers Laboratories (France) and were allowed to acclimatize to the animal facility for at least one week before any treatment. Thy-Tau22 or APPxPS1 transgenic colonies (C57Bl/6 J genetic background) were obtained by crossing heterozygous males with C57Bl/6 J WT females. All animals were housed in a pathogen-free facility at 5 to 6 animals per cage (Techniplast Cages 1284 L), with ad libitum access to food and water in a 12/12-h light-dark cycle and maintained under a constant temperature of 22 °C.

For treatment, animals were randomly distributed and **RPEL** was provided in the drinking water at a final concentration of 0.5 and 1 mg/kg, ie 12.5 µg/mL for drinking solutions taking into account an average weight of 25 g/mouse drinking 4 mL/day. Drinking bottles were changed once per week as aqueous solutions of **RPEL** were stable for more than one week, and the volume consumed was measured throughout the treatment period. Food consumption and body weight were also assessed. In WT animals, a pilot study of drug treatment was performed for one month to establish the innocuousness of **RPEL** treatment, based on physiological, social and behavioral assessments. Thy-Tau22 or APPxPS1 males were treated for 4 months, starting at 3 months of age.

2.12. Spatial memory assessment using the Y-maze and Morris water maze

Before any behavioral test, exploratory behavior and locomotion were evaluated in treated and untreated animals in an Open field (OF) 25 cm × 25 cm arena. Four acquisitions in 4 joined arenas were performed simultaneously. Each mouse was placed in the arena and allowed to explore for at least 5 min. Parameters including distance, speed and velocity were acquired by video recording using EthoVision video-tracking equipment and software (Noldus Information Technology, Paris, France) in a dedicated room. Anxiety, which could interfere with the memory test, was evaluated using the elevated plus maze (EPM). Mice were placed in the center of a plus-shaped maze consisting of two 10-cm-wide open arms and two enclosed arms elevated to 50 cm from the floor. Locomotion, distance, speed and velocity were measured, as well as the number of entries into each arm, time spent in open versus closed arms, percentage of open arm entries and time spent in the open arms during a 5 min test.

2.13. Y-maze

Short-term memory was tested on a Y-maze. The Y-maze consists of three enclosed arms surrounded by spatial clues. One arm was closed off during the learning phase. Each mouse was randomly positioned in the center or in one of the two open arms. Mice were allowed to explore the maze for at least 5 min. During 2 min of retention time, the closed arm was opened and the mouse was re-placed in the starting arm. The previously closed armed was named the “new arm” and the third arm was named the “other arm”. Parameters - total distance travelled, velocity, alternation between the arms, entries into the new, starting or other arm - were measured over 5 min. The short-term memory test was considered successful when the proportion of entries into the new arm was significantly higher than into the other two.

2.14. Morris water maze

Spatial learning and memory abilities were assessed in a standard hidden-platform acquisition-and-retention version of the Morris water maze task (Jeugd et al., 2011). A 90-cm circular pool was filled with water opacified with nontoxic white paint and kept at 21 °C. A 10-cm round rescue platform was hidden 1 cm beneath the surface of the water at a fixed position. Four positions around the edge of the tank were arbitrarily designated as the four cardinal points (North, East, West and South) in order to divide the pool into four quadrants. The “target” quadrant (T) contained the rescue platform, and was surrounded by the two “adjacent” quadrants (Right: R; Left: L) and an “opposite” quadrant (O). In the acquisition trial, each mouse was given four swimming trials per day with at least 10 min of inter trial interval, for four consecutive training days. The start position was pseudo-randomized across trials. Mice that failed to find the hidden platform within 2 min were manually positioned on the platform. They were allowed to remain on it for 15 s before being put back into their cages. The time required to find the hidden rescue platform (escape latency) was used as a spatial learning index and was recorded using the Ethovision XT video tracking system (Noldus France). Swimming speed and total distance were also measured. The hidden platform was removed 72 h after the acquisition phase, and spatial memory was evaluated in a 90 s probe trial. The proportion of time spent in the target quadrant vs. the other quadrants (R, L and O) was considered as a spatial memory index.

2.15. Mouse brain samples

After behavioral assessment, blood was collected in 1.5 mL polypropylene tubes (Eppendorf, France) and mice were sacrificed by cervical dislocation to avoid any modifications due to anesthesia (Le Freche et al., 2012). Hippocampi and cortices were dissected and snap-

frozen in 1.5 mL tubes (Eppendorf). Tissue was homogenized in Tris-HCl buffer (10 mM pH 7.4) containing 320 mM sucrose plus protease inhibitors (Complete mini EDTA-free, Roche) and sonicated and spun at 12,000 ×g for 10 min at 4 °C. The supernatant was recovered; protein concentration was measured with the BCA Protein quantification assay kit (Pierce) according to the manufacturer's instruction. The supernatant was further processed for biochemical analyses or stored at −80 °C. The same lysis buffer was used for 1D or 2D gels. A solution containing 7 M urea, 2 M thiourea and 2% SDS was added to equal amounts protein in Tris buffer, and sonicated at 60 Hz for 30 pulses.

2.16. Analyte mouse brain extraction

50 mg of brain were defrosted in Eppendorf tubes purchased by GE Healthcare (Grinding Kit). 500 µL of HCl 1% were added and the mixture was crushed until obtaining an homogenate. The appropriate quantity of internal standard was added. The Eppendorf tubes were centrifuged at 14000 tr/min for 10 min at 4 °C. 450 µL of the supernatant were placed on polypropylene tubes and 4.5 mL of acetonitrile at −20 °C were added. Tubes were stirred for 30s and placed 1 h at −20 °C for proteins precipitation. The tubes were centrifuged for 10 min at 4 °C at 4000 tr/min and the supernatant was evaporated under N_2 at 50 °C. The residue was dissolved in acetonitrile and evaporated once again. The final residue was dissolved in 200 µL of methanol, filtrated and placed in polypropylene vials for analysis.

2.17. Analyte mouse plasma extraction

50 µL of plasma were homogeneised in Eppendorf tubes purchased by GE Healthcare (Grinding Kit). 25 µL of internal standard (10 nM in cooled methanol) and 225 µL of cooled methanol with 1% formic acid were added. The mixture was vortexed for 10 s three times then cooled to −20 °C during 20 min. The tubes were centrifuged for 10 min at 4 °C at 10000 g and the supernatant was evaporated under N_2. The final residue was dissolved in 50 µL of methanol and placed in polypropylene vials for analysis.

2.18. SDS-PAGE and western blotting

To analyze the carboxy-terminal product of APP metabolism, equal quantities of proteins (20 µg per lane) were loaded onto a 16.5% Tris-Tricine polyacrylamide Criterion XT gel using Criterion XT Tris-Tricine Buffer (Bio-Rad). The XT Tricine buffer was precooled to 4 °C and the electrophoresis tank was placed on ice. Electrophoresis was carried out at 200 V for 65 min. Proteins were transferred to a nitrocellulose membrane of 0.2 µm pore size (G&E Healthcare) at a constant current intensity of 2.5 mA/cm^2 using a Criterion liquid transfer unit (Bio-Rad). For the western blotting of other proteins, SDS-PAGE was performed according to the manufacturer's instructions using a Bis-Tris 4–12% gradient acrylamide gel (NuPage® Bis-Tris PreCast 12 wells, Life Technologies). Apparent molecular weights were calibrated using molecular weight markers (Novex and Magic Marks, Life Technologies). Electrophoresis was performed under a continuous tension of 100 V/per gel for 1 h. Proteins were reversibly stained with Ponceau Red to check the quality and efficacy of protein transfer. For western blot analysis, the membranes were blocked in 25 mM Tris-HCl pH 8.0, 150 mM NaCl, 0.1% Tween-20 (*v*/v) (TBS-T) and 5% (*w*/*v*) of skimmed milk (TBS-M) for 30 min and then incubated overnight at 4 °C with the primary antibody. The nitrocellulose membrane was rinsed three times for 10 min each in TBS-T with gentle shaking. The membrane was then incubated for 1 h at room temperature with the secondary antibody (peroxidase-labeled goat anti-rabbit IgG (H + L chains), Vector Laboratories). The immunoreactive complexes were visualised using the ECL™ Western Blotting kit and image acquisition was performed with the LAS-3000 Luminescence Image Analyzer (FujiFilm Lifesciences) or by exposure to Amersham Hyperfilm ECL™ (G&E healthcare). Digitized images were processed with ImageJ Software (NIH).

2.19. Two-dimensional gel electrophoresis

Two-dimensional gel electrophoresis was performed as recently described (Fernandez-Gomez et al., 2014). Briefly, cells were rinsed once with PBS and lysed in UTS buffer (7 M urea, 2 M thiourea, 2% SDS) and sonicated at 60 Hz for 30 pulses. Lysates containing 50 µg of proteins were precipitated with methanol/chloroform, and the pellet dissolved in 2D buffer [urea 7 M, thiourea 2 M, 4% CHAPS, and 0.6% Pharmalytes 3–10 (G&E healthcare)]. Immobilized pH 3–11 gradient strips (Immobiline™ DryStrip of 11 cm; G&E Healthcare) were rehydrated with 200 µL of buffer containing a final amount of 50 µg of protein and isoelectric focusing was achieved with an IPGPhor III apparatus (G&E Healthcare) according to the manufacturer's instructions. The strips were layered onto a Criterion XT™ Precast 4–12% Bis-Tris Polyacrylamide Gel (Bio-Rad) and run under a constant tension of 100 V.

2.20. Quantification of secreted Aβ in cell media and Tau in mouse plasma

Conditioned media were briefly centrifuged at 200 g to eliminate cell debris and $A\beta_{42}$ concentration was determined using INNOTEST™ beta-Amyloid (1–42) (Innogenetics, Ghent, Belgium). $A\beta_{43}$, $A\beta_{40}$ and $A\beta_{38}$ concentrations were determined using ELISA kits (IBL, Japan) according to the manufacturer's instructions. For plasma dosage of $A\beta_{40}$ and $A\beta_{42}$, blood was recovered following a tail incision under a red heating lamp in Microvette® CB 300 LH tubes (SARSTEDT, Marney, France). The blood was spun at 4000 rpm for 15 min at 4 °C. The plasma was recovered and kept at −20 °C. For the dosage of $A\beta_{40}$ and $A\beta_{42}$ peptides, the plasma was diluted 1/5 in ELISA buffer according to the manufacturer's instructions (Life Technologies). hTau concentrations were measured using the total Tau and phospho-181 hTau Innotest® ELISA kits (Fujirebio Europe) according to the manufacturer's instructions. hTau and phospho-Tau measurements were performed using 25 or 75 µL of plasma.

2.21. Immunofluorescence

SY5Y-APP^{695WT} neuroblastoma cells were plated in cell culture chamber slides (Labtek) and allowed to grow in DMEM supplemented with 10% fetal calf serum. Treatment with compounds was performed following the same protocol described in the drug treatment paragraph. After 48 h, cells were fixed with 4% paraformaldehyde in 0.1 M phosphate buffer (PBS) for 15 min at room temperature. Cells were washed 3 times with ice-cold PBS and blocked with PBS supplemented with 1% BSA, then incubated with primary antibodies overnight at 4 °C in PBS-BSA, rinsed 3 times with ice-cold PBS and incubated with an FITC or rhodamine-conjugated secondary antibody (Life Technologies). The coverslips were mounted onto slides with Vectashield mounting medium with DAPI (Vector laboratories). Images were acquired with a Zeiss Apotome or Confocal light scanning microscope Zeiss LSM 710. For Apotome image acquisition, the Axio Imager was used with an optical plan-apochromat 63×/1.4 oil M27 at room temperature. For confocal, images were acquired with the same optic at room temperature and a camera PMT 32 channels (photomultiplicator) with the acquisition software ZEN 2011. All data were analyzed using Photoshop Element 6 Software (Adobe) without any modification of raw images.

2.22. Immunohistochemistry

Animals were sacrificed by cervical dislocation after the completion of behavioral tests. Brains were removed on ice in a cold room. Brain hemispheres (APPxPS1; untreated $n = 9$ and treated $n = 10$; Thy-Tau22: untreated $n = 6$ and treated $n = 5$) were post-fixed for 7 days in PBS with 4% paraformaldehyde, immersed in PBS with 20% sucrose for

24 h and finally frozen and stored at −80 °C until use. Serial free-floating coronal sections of 40 µm thickness were obtained using a cryostat (Leica Microsystems GmbH, Germany). Amyloid deposits or neurofibrillary tangles were visualized after free-floating immunohistochemistry using the antibodies AT8 (Pierce MN-120, against pS202/T205, 1/200), AT100 (Pierce MN-1060, against pT212/S214, 1/400) and 4G8 (Covance, 1/500, according to the manufacturer instructions), followed by diaminobenzidine labeling. Sections were then mounted on gelatin slides. The labeled surface as a proportion of the entire brain region surface was quantified (Mercator software; Explora Nova) in the hippocampus and cortex by two investigators blind to treatment group, on a minimum of 5 slices per animal separated by 400 µm. A threshold intensity was set and kept constant and the number of pixels, representing labeling density, was determined for all groups of mice.

2.23. Experimental design and statistical analysis

For animal experimentation, males were housed at 5 to 6 animals per cage and randomly distributed for RPEL treatment. The experimental design and number of animals per treatment condition were approved by the local ethics committee (n°342,012). For behavioral tests a minimum of 5 and a maximum of 9 animals per conditions were included. A number was attributed to each animals and experiments were made blind without knowing to which experimental condition each animal was belonging. For statistical analysis behavioral test results were re-organized according to each treatment condition and WT were compared to transgenic animals. For biochemical analyses, 5 animals per conditions were included. Duplicates were made for ELISA and western-blot analyses. A minimum of 5 brain slices per animals were analyzed. Quantification of labelling was averaged for each animal and a minimum of 5 animals per experimental condition were compared. Results were reported as means ± SEM. Differences between mean values were evaluated using the Student's *t*-test and one way-ANOVA followed by a post hoc Fisher's LSD test, using GraphPad Prism 6 Software. P values < .05 were considered to indicate a significant difference.

3. Results

3.1. Design of compounds

We previously developed *N,N′*-disubstituted piperazine compounds (MSBD, Fig. 1A) for the design of amyloid metabolism modulators as chloroquine (CQ) derivatives (Melnyk et al., 2006; Melnyk et al., 2015). Compound **AZP2006** (**29** in Melnyk et al. (2015), R = benzimidazole) is currently under development as a potential anti-Alzheimer drug candidate. With the aim of developing a composite drug for the treatment of the symptoms of AD, we substituted the R group of these compounds with two well-known AChE inhibitors, tacrine and rivastigmine, to create two constructs, named **RPEL** and **MAG** respectively (Fig. 1A) (Melnyk et al., 2006; Melnyk et al., 2015). The rationale for using AChE inhibitors relies on the hypothesis that the substitution of *N,N*-disubstituted piperazine preserves the activity of our compounds, respect structure-activity relationships of our family of MSBD compounds as well as the AChE inhibition, having in mind that the latter does not occur inside the cell. Chemically more simple dimethyl carbamate moiety was chosen for **MAG** compound. We therefore first verified that **RPEL** and **MAG** could preserve the AChE inhibitory activity of their adducts by docking both molecules with the catalytic pocket of hAChE (Fig. 1B) and *in vitro* measurement of the activity. Aromatic part of **RPEL** superimposed perfectly with tacrine and interacts with Trp86 (Fig. 1B left). Carbamate part of **MAG** interacts with catalytic triad (Ser203, Glu334 and His447) as rivastigmine (Fig. 1B right). Both **RPEL** and **MAG** present their piperazine chain along the gorge and interact with AChE peripheral site (Trp286) as donepezil.

In silico prediction of ADME and BBB permeability of compounds RPEL and MAG were performed using ACD/ADME Suite 5.0 software. Both compounds were predicted to have good bioavailability (between 30 and 70%) and a sufficient BBB permeability for CNS drug candidates.

3.2. In vitro evaluation

3.2.1. Acetylcholinesterase activity

The hAChE inhibitory activity of **RPEL** and **MAG** was then evaluated *in vitro* using tacrine and rivastigmine as reference compounds (Ellman et al., 1961). **RPEL**, with an IC_{50} of 0.84 nM, was 135 times more potent as an AChE inhibitor than tacrine (IC_{50} = 115 nM) while **MAG** was 85 times more inhibitory than rivastigmine (**MAG** IC_{50} = 398 nM versus rivastigmine IC_{50} = 33,800 nM). As a comparison, compounds bearing only a *N,N′*-disubstituted piperazine chain provide IC_{50} higher than 30 µM (compound **2** or **MAF** in supplementary information). Substitution of the two AChE inhibitors with MSBD chain allows a better interaction with AChE and thus a real boost in efficacy.

3.2.2. APP metabolites and Aβ production

APP metabolism is the target of N,N′-disubstituted piperazine compounds, we next investigated the consequences of **RPEL** or **MAG** treatment on APP metabolism. First, we verify that no cytotoxicity could be measured up to 10 µM (see supplementary Fig. S1). The proteolytic processing of APP consists of a sequence of cleavages involving either α- or β-secretase followed by γ-secretase cleavage (De Strooper, 2010). The α-secretase cleaves APP within the Aβ sequence, producing a soluble fragment (sAPPα) and a carboxy-terminal fragment (CTFα), and precludes Aβ production (Vingtdeux and Marambaud, 2012). The β-secretase cleaves APP at the first amino acid residue of the Aβ sequence, producing a soluble fragment (sAPPβ) and a transmembrane carboxy-terminal fragment (CTFβ), which is further cleaved by γ-secretase to produce Aβ peptide (Pardossi-Piquard and Checler, 2012) (Schematic representation on Fig. 2A). Following **RPEL** treatment of SKNSH-SY5Y APP^{695WT} neuroblastoma cells with concentrations ranging from 0.5 to 10 µM, the cell content of APP was not different from the control condition (Fig. 2B). We next analyzed soluble-APP fragments (APPs) shedded by either α- or β- secretase. The global sAPP content was reduced by 20% at 10 µM of **RPEL** (Fig. 2B) but neither **RPEL** nor **MAG** significantly modified the shedding of APP (Fig. 2B). The carboxy-terminal fragments of APP (APP-CTFs), which are transmembrane fragments resulting from α- or β- secretase cleavage, were also analyzed. At the basal level, the APP-CTFs observed were mostly the αCTFs. βCTFs were only observed on exposure to saturating concentrations of the drugs and using a specific antibody detecting the Aβ epitope 5–15 (Fig. 2C). The APP intracytoplasmic fragment (AICD) which is released following the endopeptidase activity of γ-secretase on APP-CTFs was detected and measured following long-time exposure. At 5 µM of **RPEL**, the amount of APP-CTFs was similar to that observed with 5 µM of CQ (Fig. 2D). Notably, the western blot profiles of APP-CTFs were very similar following CQ and **RPEL** treatment. Moreover, both **RPEL** and **MAG** increased the basal level of AICD up to 8-fold (Fig. 2D). Tacrine was also evaluated alone as well as a simple MSBD compound or the mixture of both compounds. The western blot profiles of APP-CTFs were very similar to that of CQ or control and showed lower efficiency when compared to **RPEL** (see supplementary Fig. S2). Thus, **RPEL** activity could not be explained by either tacrine or the MSBD alone or the simple addition of both effects.

We next measured the effect of both **RPEL** and **MAG** on Aβ production. Following βCTF cleavage of APP at the ε-site by the endopeptidase activity of γ-secretase, the resulting fragment is processed by the exopeptidase activity of γ-secretase to release the Aβ peptides ($Aβ_{38}$, $Aβ_{40}$, $Aβ_{42}$ and $Aβ_{43}$ species) (Acx et al., 2014). Compounds modulating such proteolytic processing can lead to a preferential activation or repression of one of the two exopeptidase pathways or

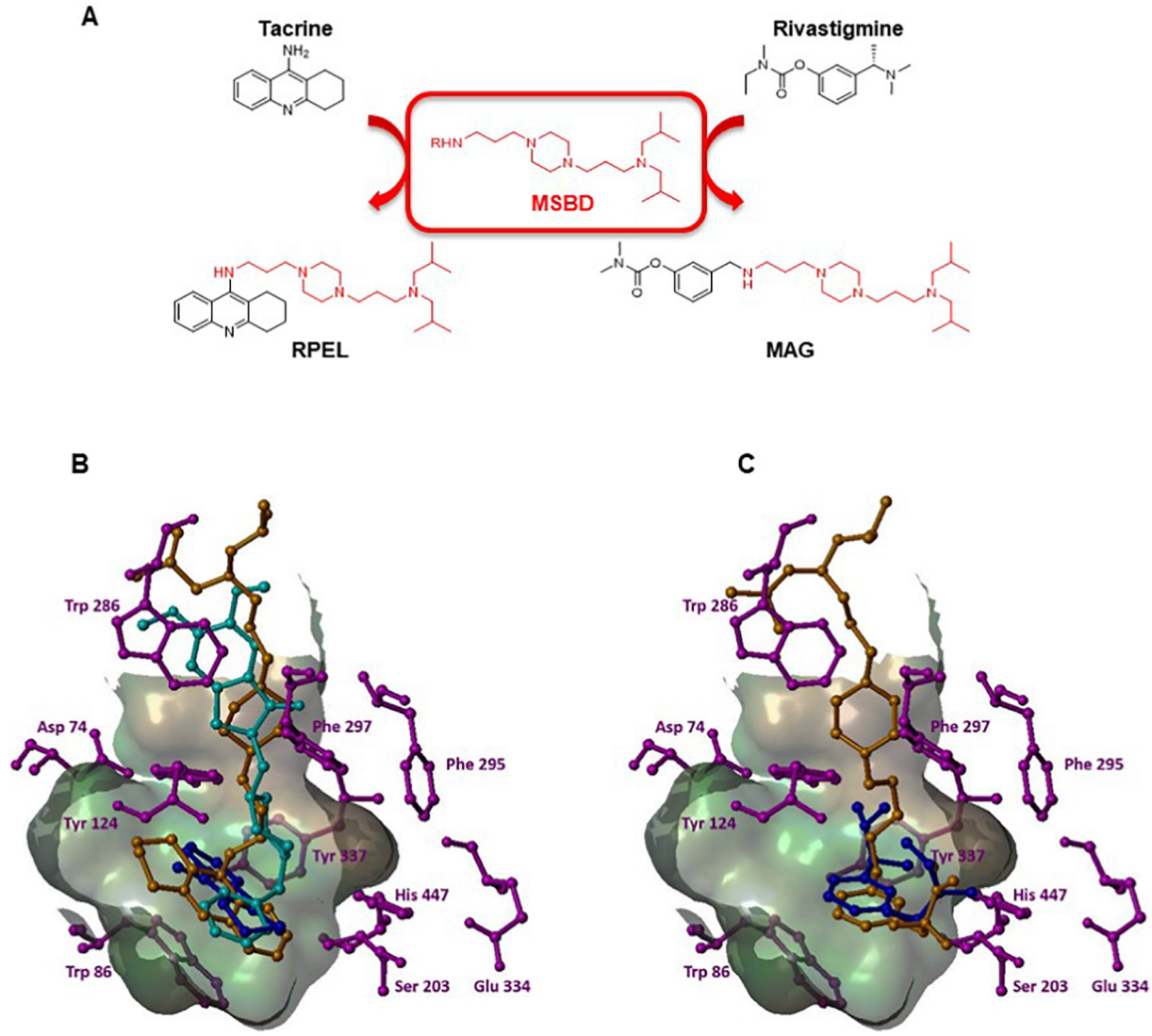

Fig. 1. Chemical structures and probable binding modes of RPEL and MAG at human acetylcholinesterase. A. Chemical structure of **RPEL** and **MAG**. The topographical formula of **RPEL** and **MAG** results from the linking of tacrine and rivastigmine respectively to the N,N′-disubstituted piperazine pharmacophore (Melnyk et al., 2006; Melnyk et al., 2015). B. Left: Superposition of the predicted binding mode of **RPEL** (in brown), tacrine (blue) and donepezil (cyan) within the active site of hAChE. Right: Superposition of the predicted binding mode of **MAG** (in brown) and rivastigmine (blue) within the active site of hAChE. **RPEL, MAG** and structures were docked within the known binding site of hAChE (PDB 4EY7) using GOLD software. Important amino acid residues (in pink) are indicated. (For interpretation of the references to color in this figure legend, the reader is referred to the web version of this article.) (For interpretation of the references to colour in this figure legend, the reader is referred to the web version of this article.)

preferentially repress the release of long forms of Aβ peptides. Therefore, we quantified the amount of $A\beta_{38}$, $A\beta_{40}$ and $A\beta_{42}$ (Fig. 2E). Notably, the amount of $A\beta_{38}$ and $A\beta_{42}$ was significantly reduced to more than three-fold after treatment with 0.5 μM of **RPEL**. In contrast, at the same **RPEL** concentration, the amount of $A\beta_{40}$ was only reduced by half. A similar trend was obtained with **MAG** although the effect was 10 times less pronounced (Fig. 2E). These results suggest that both **RPEL** and **MAG** have a modulatory effect on γ-secretase activity, repressing the $A\beta_{42}$-producing pathway to a greater extent than the $A\beta_{40}$-producing pathway. This phenomenon is also illustrated by a dose-dependent reduction of the $A\beta_{42/38}$ ratio whereas the $A\beta_{43/40}$ ratio is almost unchanged (see Supplementary Fig. S3). These results were verified by western blot analysis of the release of Aβ peptides into the cell medium (Fig. 2F). Tacrine alone, a simple MSBD compound or the mixture of both compounds were also evaluated. The Aβ concentrations remained unchanged even at 10 μM (see Supplementary Fig. S2). To further assess whether γ-secretase activity was directly modified by **RPEL** or **MAG**, the *in vitro* cleavage of APP-CTFs into Aβ and AICD as well as the cleavage of ΔE Notch (Notch lacking the extracellular domain) into the Notch intracellular domain (NICD) were investigated (Fig. 2H). The γ-secretase inhibitors DAPT and L685,458 alleviated both AICD and NICD production (Fig. 2H) whereas neither **MAG** nor **RPEL** treatment modified the *in vitro* release of AICD (Fig. 2F) or NICD (Fig. 2H).

The expression of the β-secretase BACE1 was then analyzed by western blotting. The increased quantity of βCTFs following treatments was not related to change of BACE1 protein levels; this, also suggests that **RPEL** and **MAG** have no inhibitory effect on lysosome-dependent BACE1 degradation (Fig. 2G). These results suggest, overall, that the pharmacological effects of **MAG** and **RPEL** on APP metabolism do not stem from a direct modulation of the proteolytic activities of secretases.

Thus, we showed that mixed compounds upsurge APP metabolites and decrease Aβ production without a direct effect on secretases. Moreover, the **RPEL** or **MAG** activity is not simply explained by the activity of the separate moieties.

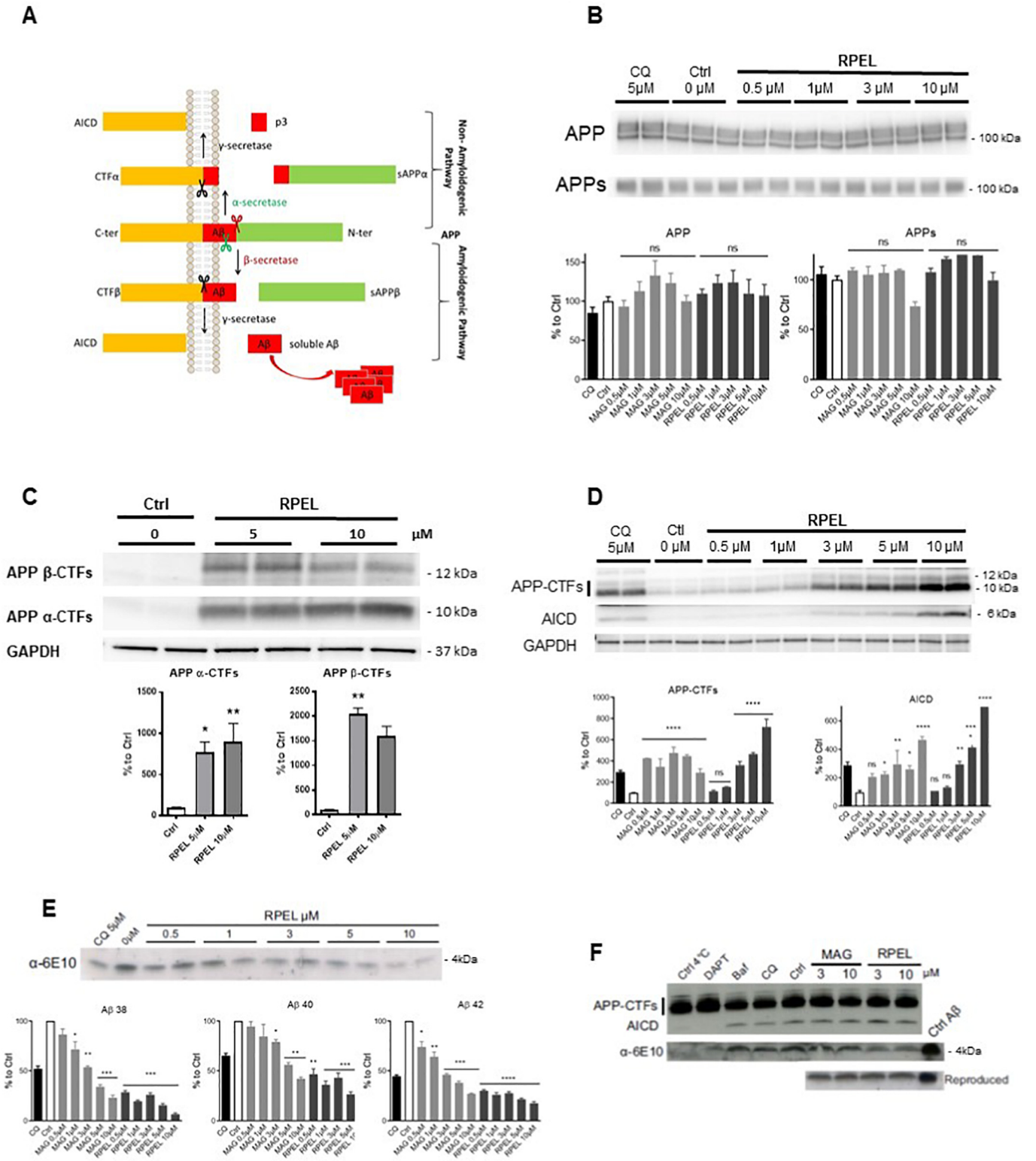

(caption on next page)

Fig. 2. RPEL promotes APP-CTFs and AICD accumulation and reduces Aβ production through a γ-secretase-independent mechanism. A. Schematic representation of APP metabolism B. Full-length APP, but not APP,s accumulate in a dose-dependent manner following **RPEL** and **MAG** treatment. SKNSH-SY5Y APP695 neuroblastoma cells were treated with 5 μM CQ or concentrations ranging from 0.5 to 10 μM of **RPEL** for 24 h. Levels of full-length APP were determined following western blotting using an APP-Cter-C17 polyclonal antibody. Levels of total APPs were determined in the medium after western blotting using the 8E5 monoclonal antibody. APP levels are not significantly diminished by **RPEL** treatment. C. The increase of both α- and β-carboxy-terminal fragments of APP in SY5Y-APP695WT treated with **RPEL**. SY5Y-APP695WT cells were treated with 5 or 10 μM of **RPEL** for 24 h. Proteins were resolved by SDS-PAGE and β-CTFs were detected using 6E10 monoclonal antibody raised against the Aβ epitope 5–15. The APP-C17 antiserum was used to labeled the α-CTFs. D. APP-CTFs and AICD accumulation in the presence of **RPEL** or **MAG**. SKNSH-SY5Y APP695 protein lysates were resolved using Tris-Tricine gels. APP-CTFs and AICD were detected with an APP-Cter- C17 antiserum. E. **RPEL** reduces the amount of Aβ peptides released without affecting BACE1 expression or γ-secretase endoprotease activity. $Aβ_{38}$, $Aβ_{40}$, and $Aβ_{42}$ concentrations are diminished in a dose-dependent manner after **RPEL** or **MAG** treatment. SKNSH-SY5Y APP695 cell medium was recovered 24 h post-treatment and Aβ concentrations were determined by ELISA. Although the calibration curve of the ELISA kits was constructed with the media containing **RPEL** or **MAG**, a western blot of Aβ released into the medium was performed with the pan-Aβ 6E10 antibody. **F.** Ex cellulo APP-processing γ-secretase is unmodified by **MAG** and **RPEL**. The release of AICD and Aβ peptides was evaluated by western blotting following incubation of total membrane extracts of SKNSH-SY5Y APP695 at 37 °C for 6 h in the presence or absence of selective γ-secretase inhibitor DAPT (200 nM), Baf (100 nM) or 3 or 10 μM of **MAG** and **RPEL**. APP-CTFs and AICD were immunolabeled with an APPCter-C17 antiserum and Aβ peptides with the N-terminal 6E10 monoclonal antibody. As a control for Aβ peptide labeling, 10 ng of $Aβ_{42}$ peptide was also loaded (Ctrl Aβ lane). The effect of **MAG** and **RPEL** on in vitro Aβ production is shown twice (Reproduced). G. Unaltered BACE1 expression. The total concentration of full-length BACE1 protein was determined by western blotting. H. SKNSH-SY5Y APPWT695 cells were transiently transfected with a eukaryotic DeltaE Notch (Notch lacking the extracellular domain)-expressing vector, and after 24 h, cells were treated with the indicated concentration of the γ-secretase inhibitor L685, 5 μM of CQ or 3 or 10 μM of either **MAG** or **RPEL**. Protein extracts were prepared 24 h post-treatment. DeltaE Notch and NICD were labeled with an antibody against c-myc, which binds to them. GAPDH staining was used to verify the protein amounts loaded and used to normalize changes in expression. Histograms represent means ± SEM of three individual experiments and values are expressed as the percentage of control levels. Statistical differences were calculated by One-way ANOVA followed by a post hoc Fisher LSD test. * $p < .05$, ** $p < .01$, ***$p < .001$.

3.2.3. Autophagy modulation

Since APP metabolism and the autophagy-lysosomal degradation pathway are tightly linked (Nixon, 2013) and BACE1 degradation occurs through a lysosome-dependent mechanism (Ye and Cai, 2014), we investigated whether autophagic flux was modified by **RPEL** or **MAG** (Fig. 3A and B). Our previous study suggested that the *N,N′*-disubstituted piperazine pharmacophore structure may act on lysosomes (Melnyk et al., 2015). Indeed, its action is similar to that of chloroquine (CQ), a lysosomotropic compound, and Bafilomycin A1 (Baf), a potent inhibitor of the autophagy (Jiang and Mizushima, 2015), which is a catabolic cellular process that is necessary for maintenance of cell protein homeostasis and possibly also deficient in several neurodegenerative diseases including AD (Nixon, 2013). Early-, intermediate- and late-stage autophagic flux markers were analyzed under normal growth conditions.

RPEL treatment induced the accumulation of Beclin 1 and p62 (Fig. 3A) as well as causing an increase in the number of p62-positive vesicles and the formation of large LC3-positive autophagosomes (Fig. 3B). Beclin 1 expression is known to be downregulated in AD (Pickford et al., 2008). In contrast, Beclin 1 overexpression activates autophagy and positively contributes to intra-neuronal aggregate clearance (Spencer et al., 2009). Next, we analyzed the LC3-dependent autophagic pathway. Following the activation of autophagy, LC3-I is coupled to a phosphatidylethanolamine residue, leading to LC3-II, which subsequently associates with the autophagosome membrane. Mature autophagosomes fuse with lysosomes, which leads to the degradation of their contents. Both CQ and Baf inhibit this late stage and thus the autophagic flux. Following treatment of SY5Y-APP^{WT} cells with CQ and Baf, a robust accumulation LC3-II and numerous LC3-positive autophagosomes were observed (Fig. 3A and B). In sharp contrast, only a modest accumulation of LC3-positive autophagosomes and a diffuse cytosolic signal were observed, following **RPEL** treatment at 3 and 5 μM, suggesting that the autophagic flux was not completely repressed by **RPEL** (Fig. 3A, data not shown for **MAG**). Thus, we showed that mixed compounds modulate autophagy without complete inhibition.

3.2.4. Tau hyperphosphorylation and proteolysis

Modulation of the autophagy-lysosomal pathway may also impact the metabolism of the microtubule-associated protein Tau. This impaired activity of autophagy-lysosomal degradation likely contributes to AD (Inoue et al., 2012; Polito et al., 2014; Zhang et al., 2014). We therefore investigated the effects of **RPEL** and **MAG** on Tau metabolism and phosphorylation. SKNSH-SY5Y neuroblastoma cells expressing the human Tau isoform 412 were treated with 5 μM of either **RPEL** or **MAG**. Tau expression and total phosphorylation were assessed by 1D and 2D gel electrophoresis using phospho-specific and pan-Tau antibodies (Fig. 4A and B).

Tau expression was reduced following treatment with **MAG**, but was not significantly modified after **RPEL** treatment, although Tau phosphorylation at serine 199 and serine 396 was reduced in **RPEL**-treated cells (Fig. 4A). These results were corroborated using 2D-gel electrophoresis. Under control conditions, isovariants of Tau were resolved between pI 6.5 and 10.5. Following treatment with **RPEL**, a reduction in isovariants was observed at neutral pI with the Tau^{396P} phospho-specific antibody as well as with both the N- and C-terminal-directed pan-Tau antibodies (Fig. 3B α-Tau^{Nter} and α-Tau^{Cter}).

RPEL effects on Tau phosphorylation were also investigated in primary neuronal culture (Fig. 5). While Tau expression did not appear to be changed following **RPEL** treatment, Tau phosphorylation was significantly reduced at serine 396 and serine 422 in **RPEL**-treated primary neurons. These observations were comforted by 2D-gel electrophoresis where a change in the distribution of Tau polypeptides toward more positively charged isovariants was observed (Fig. 5B). Indeed, Tau isovariants are delocalized to the neutral and the basic part of the gel following **RPEL** treatment, suggesting a global reduction of Tau phosphorylation following RPEL treatment.

Together, our results suggest that **RPEL** and **MAG** modify the metabolism of both Tau and APP through a modulatory effect on autophagy-lysosomal activity. **RPEL** or **MAG** activity is proper effect unrelated to individual moietes (Tacrine or *N,N′*-disubstituted piperazine) and as *in vitro* results are more potent with **RPEL** than those of **MAG**, *in vivo* experiments were conducted with **RPEL**.

3.2.5. Stability of RPEL compound

Before *in vivo* experiments, chemical and metabolic stabilities of RPEL compound were checked. We first verify that aqueous solutions of **RPEL** were stable at room temperature for more than one week. Then, metabolic stability of **RPEL** compound was evaluated using mice liver microsomes. After one hour at 37 °C, at least 40% of **RPEL** remained in the media.

3.3. In vivo evaluation

3.3.1. Safety on wide-type mice

We verify that **RPEL** had no adverse effects after one month of treatment in WT animals (**RPEL** solubilized in drinking water, $n = 9$, males). No difference could be measured between treated or not animals on the weight, the assumption of water or the food intake. No

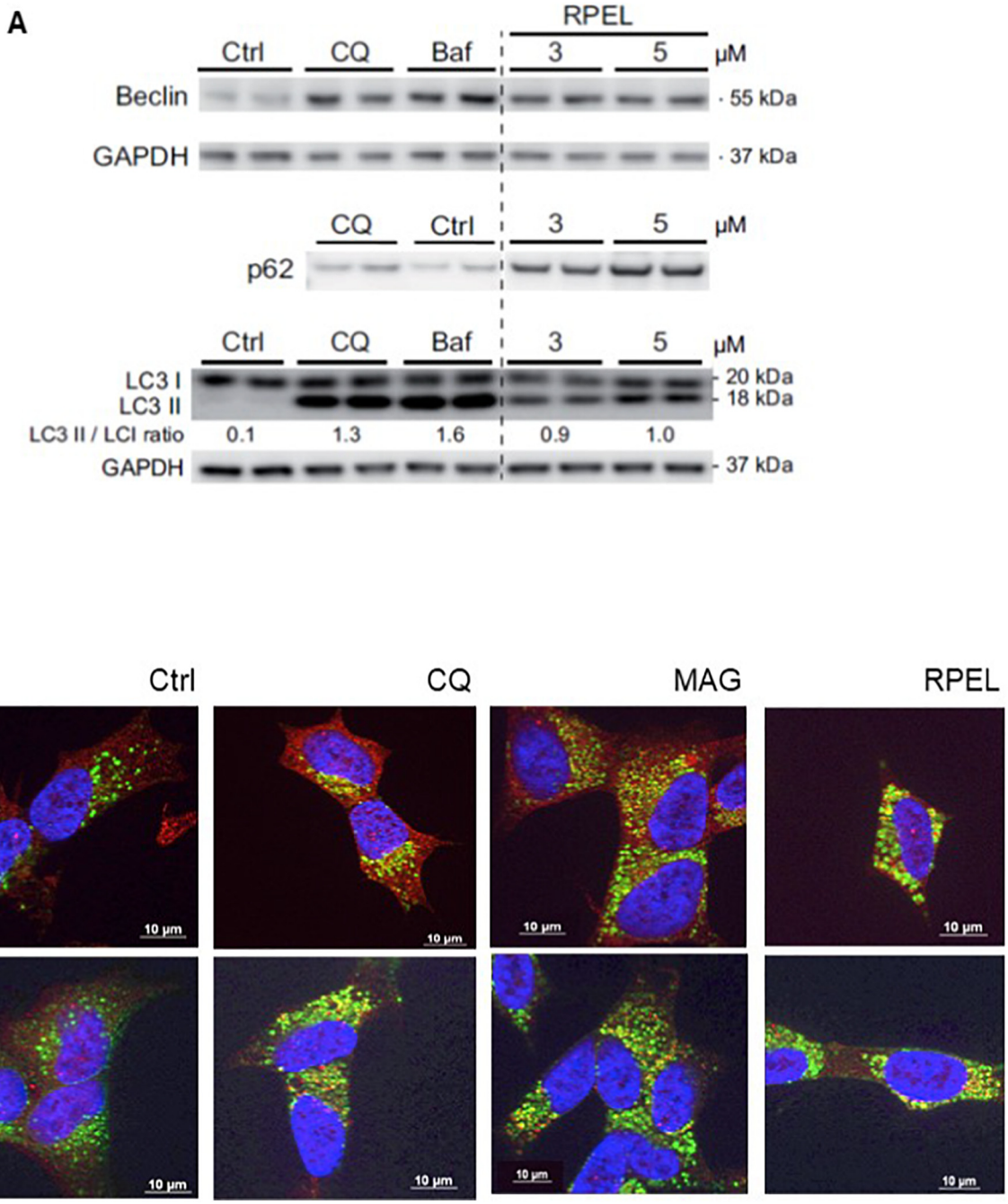

Fig. 3. RPEL does not repress autophagy. A. Comparison between **RPEL**, chloroquine (CQ) and Bafilomycin A1 (Baf) on autophagic flux. The effect of CQ 5 μM, Baf 100 nM and **RPEL** at 3 and 5 μM on protein expression of Beclin 1, p62 and LC3 were evaluated by western blotting. GAPDH labeling was used to normalize the amount of protein loaded. B. Representative confocal immunofluorescence labeling for APP (FITC-conjugated secondary antibody in green) and p62 or LC3 (Rhodamine-conjugated secondary antibody in red). Data were collected from a minimum of three individual experiments. (For interpretation of the references to colour in this figure legend, the reader is referred to the web version of this article.)

abnormal behavior, altered velocity, motility nor anxiety could be noticed. This was also confirmed with the two transgenic mice experiments. No muscular changes could be observed. We next examined whether the modulatory effect of **RPEL** on Tau and APP metabolism could have beneficial effects *in vivo*.

3.3.2. *Thy-Tau transgenic mice model of Tau pathology*

Thy-Tau22 (n = 9, males) mice were treated with **RPEL** (solubilized in drinking water). The development of hippocampal NFTs in Thy-Tau22 mice is correlated with an impairment of spatial memory (Belarbi et al., 2009; Belarbi et al., 2011; Troquier et al., 2012; Laurent et al., 2016) making the Thy-Tau22 mouse a good model in which to test the beneficial or detrimental effects of drugs. Mice were treated for four months with 0.5 and 1 mg/kg of **RPEL** (drinking water) without any difference between mice (WT or Thy-Tau22), treated or not, regarding behavior, food, and beverage intake or weight evolution. Spatial memory was subsequently assessed using the Morris water maze. Results are shown for the 0.5 mg/kg dose. All groups of animals successfully learned after the 5-day acquisition phase (Fig. 6A). In wild-type (WT) animals, independently of the treatment, animals had a significant preference for the target quadrant than for the three other quadrants (right, left and opposite, Fig. 6A). Thus, **RPEL** did not impact

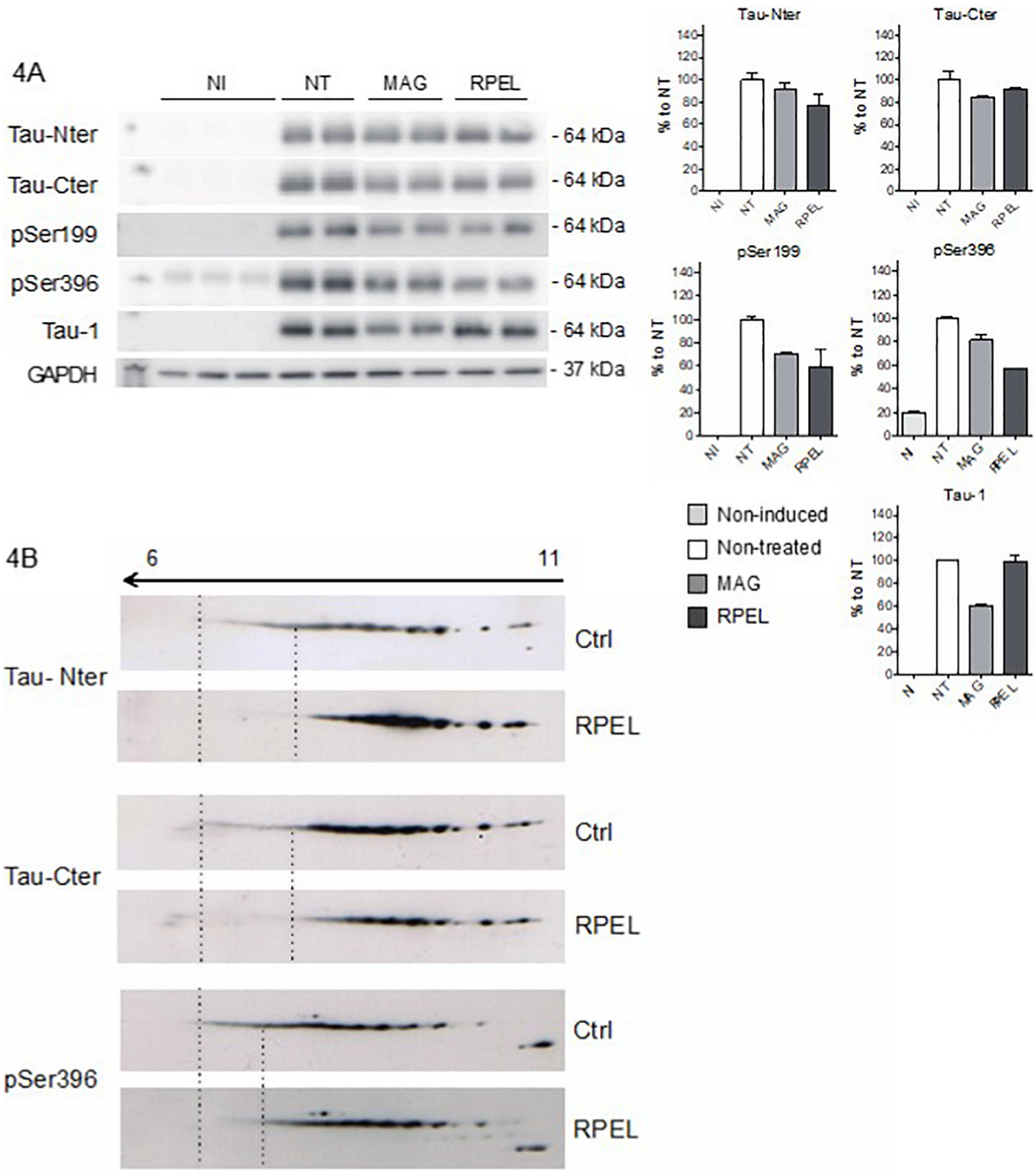

Fig. 4. Phosphorylation of Tau protein is diminished in SKNSH-SY5Y Tau^{412} expressing cells. A. **MAG** and **RPEL** treatments reduce Tau phosphorylation. A SKNSH-SY5Y Tau^{412} inducible cell line was induced (NT) or not (NI) for 24 h with tetracycline and further treated with 10 µM of **MAG** or **RPEL** for 24 h. 10 µg of protein lysates were resolved by 1D SDS-PAGE and Tau protein expression was analyzed by western blotting using two antisera against the N-terminus (Tau-Nter) and C-terminus (Tau-Cter) of the protein. Phosphorylation at serine 199 or serine 396 of unphosphorylated Tau (amino acids 199 to 208) were revealed using S199P and S396P antisera or a Tau-1 monoclonal antibody. GAPDH labeling was used to normalize the amount of protein loaded. Histograms are representative of the quantification of western-blots *B. tau* proteins are less phosphorylated following **RPEL** treatment. Total protein extracts were resolved by 2D-gel electrophoresis and Tau isovariants were revealed with antibodies to phospho-S396, pan-Tau-Nter and pan-Tau-Cter. Immobilized pH gradient strips covering isoelectric points (pI) between 3 and 11 were used, and the pI gradient indicated by the arrow above the first 2D Tau profile. Tau isovariants displayed a pI between 6 and 10.5. For each antibody used, the labeling profiles of Tau under control conditions (Ctrl) and following **RPEL** treatment (10 µM) were aligned and compared. The vertical dotted lines indicate the most neutral or acidic isovariants of Tau under the two conditions.

the cognitive performance of WT animals. Untreated Thy-Tau22 animals had no preference for the target quadrant versus the others, showing a failure to successfully complete the probe trial. In sharp contrast, **RPEL**-treated Thy-Tau22 animals succeeded in completing the probe trial after a retention period of 72 h following the learning phase and showed a significant preference for the target quadrant (Fig. 6A). The burden of neurofibrillary tangles in the hippocampal CA1 was investigated by immunohistochemistry. As shown in Fig. 6B, the average labeled surface measured after AT100 immunolabeling was significantly reduced in RPEL-treated animals, whereas no significant

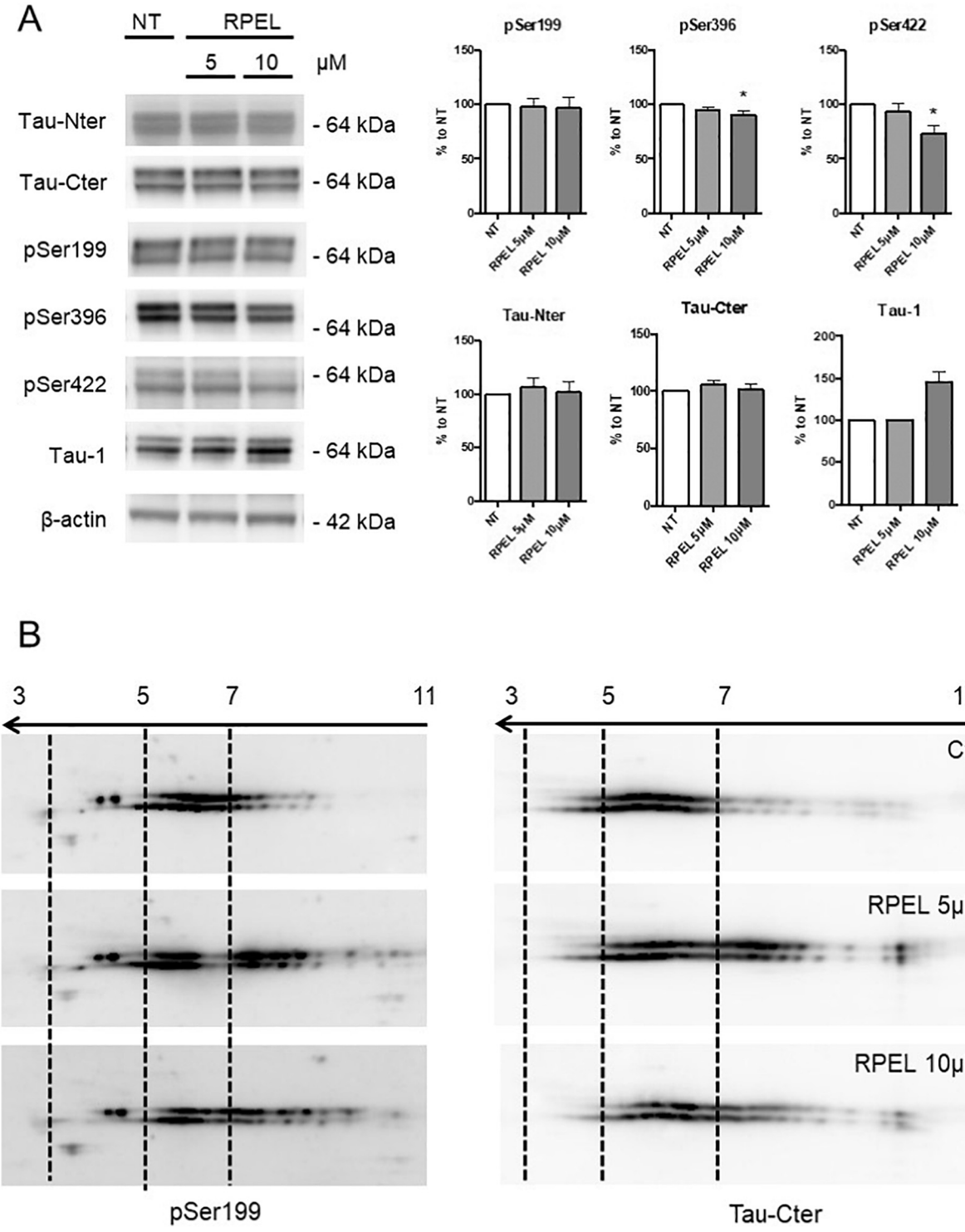

Fig. 5. Reduced phosphorylation of Tau protein in primary neuronal culture cells treated with 5 or 10 µM of RPEL. Primary neuronal culture cells at div 17 were treated for 24 h with 5 or 10 µM of **RPEL**. Total proteins were recovered and resolved by either 1D or 2D gel electrophoresis. **A. RPEL** treatment reduce Tau phosphorylation at serines 396 and 422. Mouse Tau proteins were stained with pan-Tau N-terminal (Nter) and C-terminal (Cter) antibodies as well as with several phospho-dependent Tau antibodies including pSer199, pSer 396, pSer 422 and Tau-1 which respectively recognize Tau phosphorylation at serine 199, 396 and 422 while Tau-1 recognizes Tau at an unphosphorylated epitope 198–205. Molecular weights are indicated. A Student *t*-test was applied to compare means and statistical differences were considered as significant with a $p < .05$. **B.** Accumulation of neutral and basic isovariants of Tau in **RPEL** treated primary neuronal culture cells. Primary neuronal culture cells were treated at div17 with 5 or 10 µM of **RPEL** for 24 h. Total proteins were resolved by 2D gel electrophoresis and Tau were stained using the phospho-dependant pSer199 or the pan-Tau-Cter antisera. Isoelectric points are indicated on the arrow at the top of the 2D images. The dotted line indicated the distribution of Tau isovariants in non-treated (Ctrl), and treated conditions.

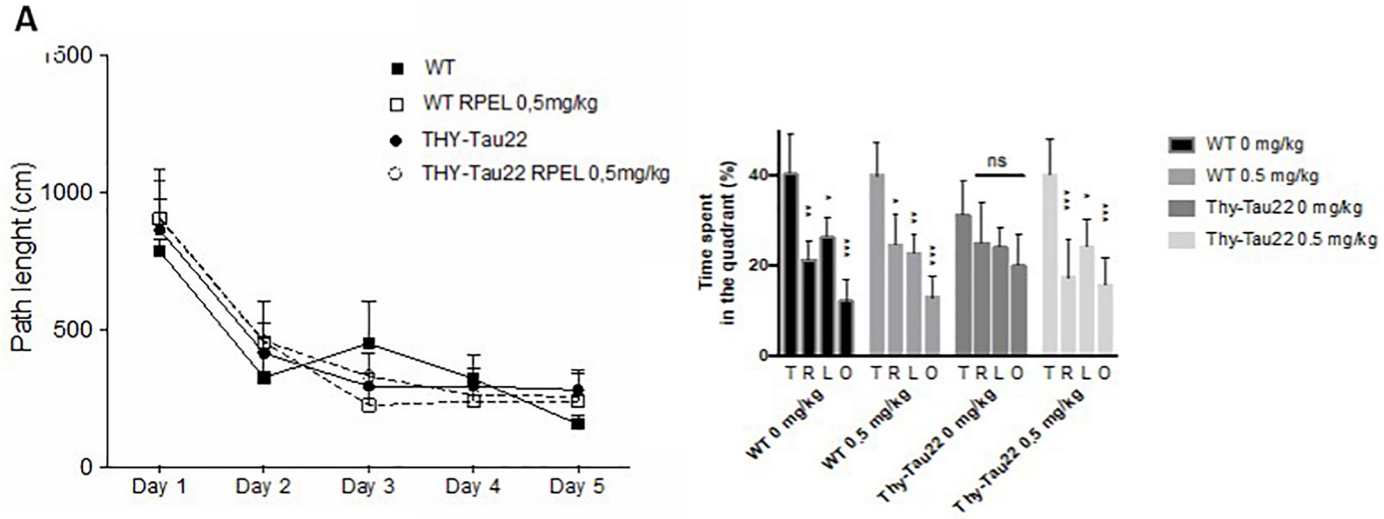

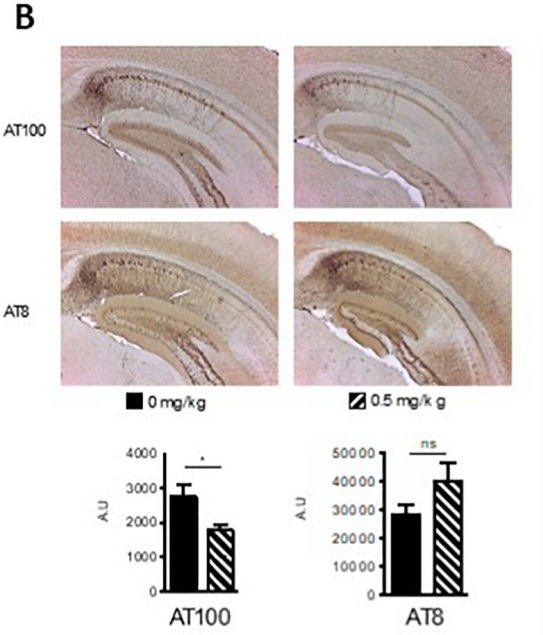

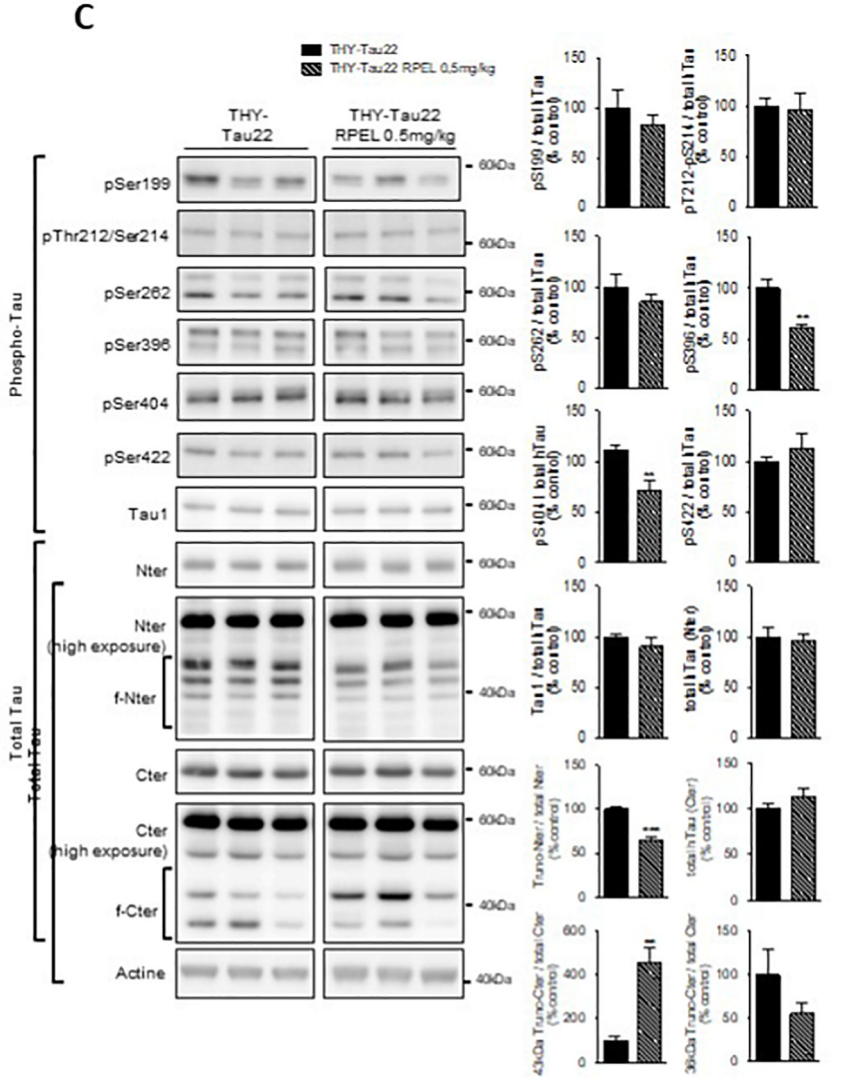

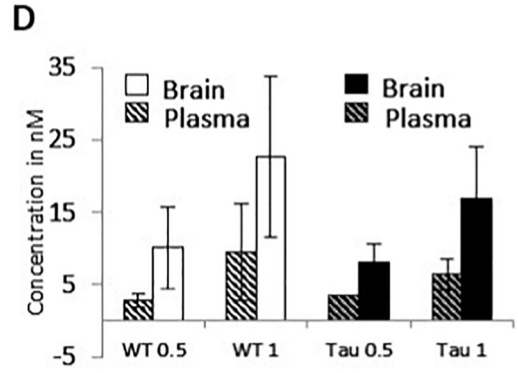

(caption on next page)

Fig. 6. RPEL improves spatial memory, reduces tau pathology and tau phosphorylation and promotes Tau catabolism in Thy-Tau22 mice. A. **RPEL** treatment of WT (open square, $n = 9$, males) and Thy-Tau22 (open circle, n = 9, males) mice (a model of neurofibrillary degeneration) with 0.5 mg/kg of **RPEL** did not modify the learning curves, expressed as path length (cm), to reach the immersed platform in the Morris Water Maze, compared to untreated animals (WT, black square, n = 9, males and Thy-Tau22, black circle, n = 9, males). Velocity and time to reach the platform were not modified in treated animals (not shown). After 5 days of training and 72 h of retention, animals were subjected to the probe test, in which the hidden platform is removed and the percentage of time spent in the target quadrant (T, where the platform was located during the learning phase) versus the other quadrants (indicated by R, L, or O for Right, Left or Opposite Quadrant) was analyzed. Histograms represent the means ± SEM ($n = 9$ animals per condition), *: $p < .05$, **: $p < .01$, ***: $p < .001$ for WT H_2O (WT 0 mg/kg) versus WT RPEL 0.5 mg/kg (WT 0.5 mg/kg) or Thy-Tau22 H_2O (Thy-Tau22 0 mg/kg) versus Thy-Tau22 RPEL 0.5 mg/kg (Thy-Tau22 0.4 mg/kg), using Tukey's Two-way ANOVA multiple comparison test followed. Abbreviations: LSD, least significant difference; SEM, standard error of the mean. B. Stereological analysis of neurofibrillary degeneration using phospho-dependent antibodies against pathological epitopes (AT100) or phospho-epitopes (AT8). The total volume (expressed in arbitrary units, A.U.) of labeling calculated from fives brain slices in $n = 5$ animals showed significantly reduced AT100 labeling (*: $p < .05$, Student's *t*-test) but no significant modification of AT8 labeling. *C. tau* phosphorylation was reduced and catabolic products increased in Thy-Tau22 animals treated with the test compounds. Western blotting of protein lysates from Thy-Tau22 mice (n = 5) or Thy-Tau22 mice treated with 0.5 mg/kg of RPEL (n = 5) were used to assess the phosphorylation of Tau at serine 199 (pSer199), serine 262 (pSer262), serine 396 (pSer396), serine 404 (pSer 404) or serine 422 (pSer422), unphosphorylated Tau consisting of residues 198–205 (Tau-1) and overall Tau expression (pan-Tau antibodies against the N-terminus (Nter) and C-terminus (Cter)). Results are represented as histograms of the mean ± SEM of the ratio of phosphorylated Tau to total Tau. The mean difference was statistically analyzed using a Student's t-test: *: $p < .05$ **: $p < .01$ ***: $p < .001$. The ratio of catabolic fragments of Tau to total Tau were also analyzed (f-Nter or f-Cter). The N-terminal ratio was significantly diminished ($p < .001$, n = 5) whereas the C-terminal ratio of the 43 kDa catabolic fragment was increased 4 fold ($p < .01$, n = 5). D. RPEL was extracted from brain and plasma and quantified thanks to LC-MS/MS procedure, showing the presence of the compound in both matrix and the accumulation of the compound in brain (WT 0.5 mg/kg $n = 6$, WT 1 mg/kg $n = 9$, Thy-Tau22 0.5 mg/kg $n = 4$, Thy-Tau22 1 mg/kg $n = 8$).

difference was observed after AT8 immunolabeling. AT100 recognized a pathological Tau epitope, suggesting that **RPEL** impacts the development of Tau pathology but not necessarily hyperphosphorylated Tau proteins. Notably, increased AT8 labeling is also in relationship to overexpression of the Tau transgene and not solely related to a modified phosphorylation rate at the AT8 site. To further explore this possibility, Tau expression and phosphorylation were investigated by western blotting (Fig. 6C). A significant reduction in Tau phosphorylation at sites 396 was observed in Thy-Tau22 **RPEL**-treated animals when compared to untreated mice, whereas other phosphorylation sites were not significantly modified (Fig. 6C). More interestingly, a 43 kDa Tau C-terminal catabolite was significantly increased whereas N-terminal catabolites were significantly decreased (Fig. 6C).

These results suggest that treatment with **RPEL** reduces the burden of Tau pathology by reducing the phosphorylation of Tau at selective phospho-sites and by increasing the catabolism of Tau, which is associated with the protection of Thy-Tau22 animals from developing spatial memory impairments. We also verified the presence of **RPEL** in mice plasma and brain. Mass spectrometry experiments using coupled HPLC to Q-Trap instrument was performed using wild type mouse as a model. Brain and plasma extraction procedures of the analyte from sacrificed mouse was carried out to quantify **RPEL** and an analytical method was validated with specificity, linearity, fidelity and accuracy criteria. Quantified results confirmed the presence and accumulation of **RPEL** in brain tissue (Fig. 6D).

3.3.3. APPxPS1 transgenic mice model of amyloid pathology

Finally, to further assess the modulatory effect of **RPEL** on amyloid pathology in vivo, APPxPS1 double transgenic animals ($n = 9$, males) were treated with 1 mg/kg of **RPEL** (solubilized in drinking water). APPxPS1 mice contain human transgenes for both APP bearing the 'Swedish mutation' and presenilin 1 (PS1) containing an L166P mutation, both under the control of the Thy1 promoter. Using the Y-maze, no alteration in short-term memory was observed in untreated or **RPEL**-treated WT animals (Fig. 7A). As already observed, treatment with **RPEL** induced no particular modification in behavior. Short-term spatial memory was impaired in APPxPS1 animals; these mice did not preferentially explore the new arm versus the other arms (Fig. 7A). In sharp contrast, in **RPEL**-treated animals, spatial memory was preserved and animals preferentially explored the new arm (Fig. 7A).

We next determined if this positive cognitive effect was associated with a modification of the amyloid burden. Stereological analysis of the hippocampus and cortex showed a significant reduction in the number of plaques following **RPEL** treatment (Fig. 7B). This reduction in the number of plaques was not associated with a change in APP expression (Fig. 7C). In contrast, the amount of APP-CTFs, as well as Aβ peptides was significantly reduced in the cortex (Fig. 7C) but not in the hippocampus. This reduction in amyloid plaque burden and Aβ peptides in brain tissue was associated with an increased plasma concentration of $Aβ_{40}$ and $Aβ_{42}$, whereas the concentration of $Aβ_{38}$ remained unchanged. Together, our results suggest that **RPEL** treatment reduces the amyloid burden and increases the plasma clearance of Aβ, with beneficial cognitive effects. These results are validated by the presence of **RPEL** in the brain (Fig. 7E).

4. Discussion and conclusion

AD is a complex disease in which multiple pathophysiological processes are spatially and temporally intermingled. Recent discoveries of genetic risks factors also support this notion since several biological pathways contribute to the development of AD. Multitarget or combined compounds may be more adapted to Alzheimer therapy. To this end, we have developed two molecules that combine AChE inhibitory activity with anti-amyloid and anti-Tau activity. The new potential drug candidates are derived from a novel class of *N,N′*-disubstituted piperazine which were originally developed in order to modify the metabolism of APP by reducing the levels of secreted Aβ peptides *in vitro* (Melnyk et al., 2015). AZP2006, the lead compound of this class is in clinical phase 1. We demonstrate herein that these two molecules effectively reduce amyloid pathology as well as the Tau pathology and moreover, one of them protects both transgenic models of these pathological mechanisms from cognitive impairments. Our results therefore demonstrate that these new multi-effect derivatives can preserve their pharmacological activity while the AChE inhibitors tacrine and rivastigmine also maintain their AChE inhibitory when covalently added to the backbone of starting *N,N′*-disubstituted piperazines. Multi-effect drug candidates from the literature, derived from tacrine, share common properties with **RPEL**, such as improved AChE inhibition and reduced Aβ release or aggregation (Chen et al., 2013; Keri et al., 2013; Munoz-Torrero, 2008). Herein, we show that their modulatory effect on APP metabolism also includes the stabilization of APP catabolites, reminiscent of an effect on endosome/lysosome modulation (Vingtdeux et al., 2007; Vorobyeva et al., 2014; Tam et al., 2014). However, this effect does not impact the global level of BACE1, whose degradation is an endosome-lysosome dependent mechanism (Ye and Cai, 2014) Moreover, our *in vitro* data further suggest that the modulatory effect takes place through a γ-secretase-independent mechanism related to the autophagic-lysosomal compartment, different from the complete blockade of the macro-autophagic flux induced by the proton-pump inhibitor Baf. The increased level of Tau C-terminal catabolites further

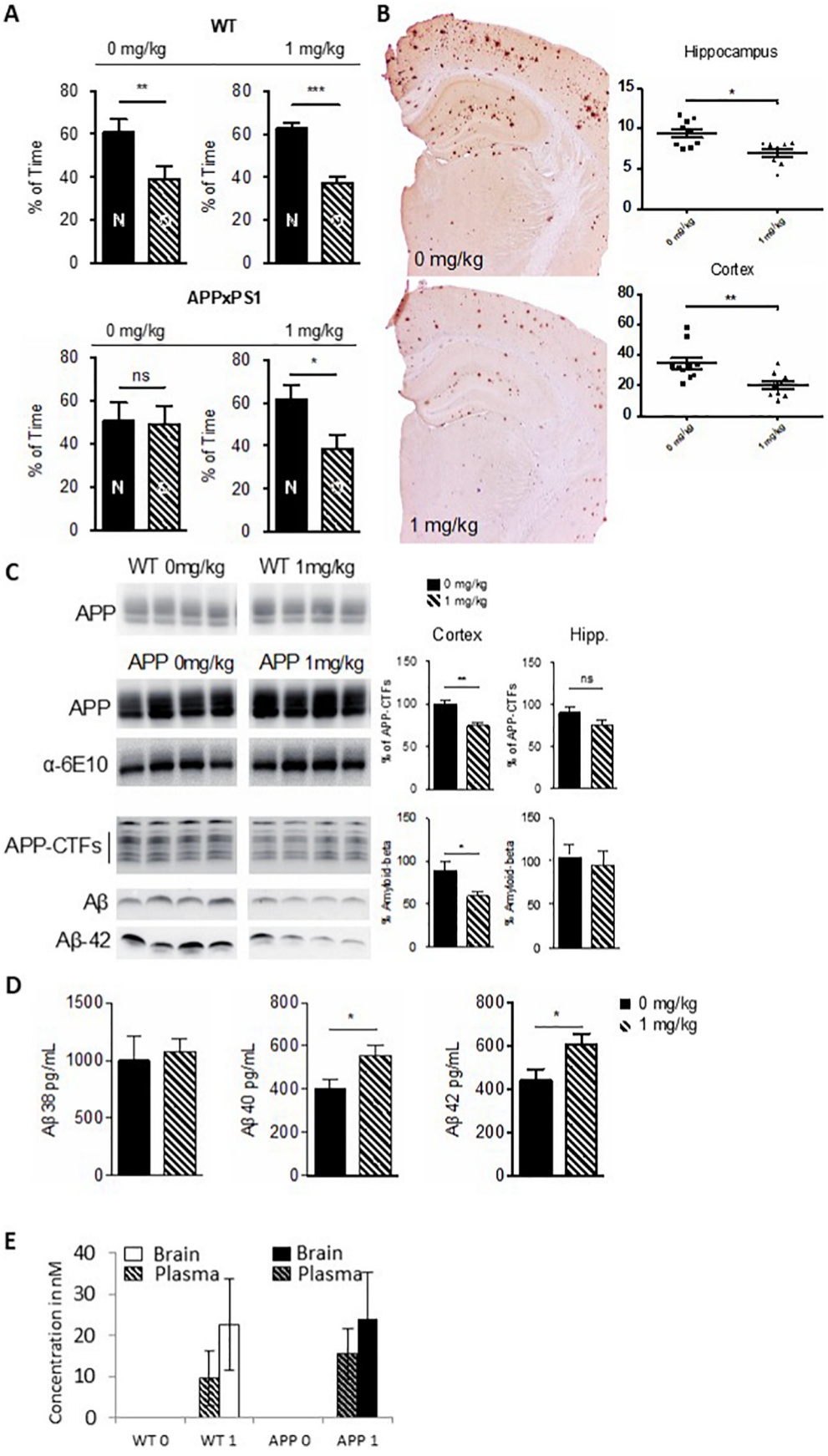

Fig. 7. *In vivo* treatment of an APPxPS1 transgenic model of amyloid pathology, with RPEL improves short-term spatial memory, reduces amyloid plaque burden and increases $A\beta_{40}$ and $A\beta_{42}$ peptide concentrations in plasma. A. **RPEL** improves short-term spatial memory in APPxPS1 mice. Histograms represent the mean ± SEM (n = 9 animals per condition, males) of the percentage of time spent in the new arm (N) versus the others (O). Statistically significant differences, *: $p < .05$, **: $p < .01$ and ***: $p < .001$ was calculated by one-way ANOVA followed by a post hoc Fisher's LSD test. **RPEL** 1 mg/kg did not improve performance in WT animals but improved short-term spatial memory in APPxPS1 animals ($p < .05$, n = 9). **B. RPEL** treatment reduces amyloid pathology in APPxPS1 mice. Amyloid deposits were labeled using the 4G8 monoclonal antibody. Histological labeling is shown for representative coronal sections of APPxPS1 mice left untreated or treated with 1 mg/kg of **RPEL**. Amyloid plaque volumes were quantified using the Explora system and means ± SEM (n = 10 slides per animal) in the hippocampus and the cortex and are represented by scatter-plots. The Student's t-test was used to analyze differences per group of animals (untreated APPxPS1: n = 9 animals, treated APPxPS1 animals: n = 10). A two-fold reduction in amyloid plaque number was observed in the cortex in APPxPS1 animals treated with 1 mg/kg of RPEL (**$p < .01$). **C.** APP metabolism was analyzed by western blotting. Full-length APP in WT animals (n = 9 untreated animals and n = 10 animals treated with 1 mg/kg **RPEL**) was labeled using the APP-CterC17 polyclonal antibody. In APPxPS1 mice, full-length APP expression was analyzed using anti-APP-CterC17 and the 6E10 monoclonal antibody, which is specific to the human epitope. APP-CTFs were labeled with the APP-CterC17 antiserum and total human Aβ or $A\beta_{42}$ peptides were labeled with the 6E10 and 21F12 monoclonal antibodies, respectively. The results of APP-CTFs and Aβ quantification are represented as means ± SEM (n = 9 animals in the untreated and n = 10 animals in the treated group). **RPEL** treatment at 1 mg/kg significantly reduced APP-CTFs (*: $p < .05$, Student's t-test) and Aβ quantities (**: $p < .01$, Student's t-test) in the cortex. **D.** Plasma concentrations of $A\beta_{40}$ and $A\beta_{42}$ but not $A\beta_{38}$ were significantly increased in APPxPS1 animals treated with 1 mg/kg of **RPEL** (hatched bars) when compared to the untreated animals (Ctrl group at 0 mg/kg, black bars). Results are reported as means ± SEM (n = 9 animals per condition). **E. RPEL** was extracted from brain and plasma and quantified thanks to LC-MS/MS procedure, showing the presence of the compound in both matrix and the accumulation of the compound in the brain (WT 1 mg/kg n = 9, APPxPS1 1 mg/kg n = 9).

supports these data. A growing body of evidence suggests that the autophagic-lysosomal compartment and lysosomal proteases, such as asparagine endopeptidase, contribute to neurofibrillary degeneration (Zhang et al., 2014; Nijholt et al., 2013; Barsuto-Islas et al., 2013). **RPEL** reduced the phosphorylation of Tau both *in vitro* and *in vivo,* but more surprisingly, it induced the accumulation of C-terminal fragments in the cell model and WT and Thy-Tau22 transgenic mice, suggesting that the Tau phosphorylation is reduced and its catabolism enhanced. Although correlative, these effects on Tau appeared to improve spatial memory in an animal model of Tau pathology. These effects are likely not due only to anti-AChE activity since other AChE inhibitors such as tacrine, rivastigmine and huperzine do not show modulatory effects on APP metabolism and Aβ production *in vitro* (data not shown). Lack of cholinergic toxicity or side-effects has to be underlined.

In conclusion, we report for the first time here that a tacrine derivative fused with the chemical backbone of an *N,N′*-disubstituted piperazine family of compounds reduces both amyloid and Tau pathologies *in vitro* and *in vivo*, and protects animal models of AD, with these pathologies, from the deterioration of cognitive function. Further investigations are needed to demonstrate and decipher the mechanism(s) underlying the modulatory effects of our two compounds on the autophagic-lysosomal pathway. In addition, as a member of the *N,N′*-disubstituted piperazine family is currently in clinical phase 1, supporting our observation that our molecules are non-toxic and could potentially find applications in neurodegenerative diseases such as Alzheimer's disease or Tauopathies, which all have the NFD process in common.

Conflict of interest

none.

Supporting information

Synthetic protocols for RPEL and MAG compounds together with ^{1}H and ^{13}C NMR, mass spectra and HPLC purity data of original compounds.

Cytotoxicity of RPEL and MAG compounds.

Cellular evaluation of Tacrine, MAF compound and the combination of Tacrine and MAF.

Effect of RPEL and MAG compounds on the secretion of Aβ peptides.

Authors contribution

David Blum: Design of the study and analysis of data.
Luc Buée: Design of the study and wrote the manuscript.
Valérie Buée-Scherrer: Analyses of biochemical data.
Raphaelle Caillerez: Histological and stereological study.
Pascal Carato: Structure activity relationship study.
Mathilde Coevoet: Cell assays.
Patrick Dallemagne: AChE inhibition assay.
Amandine Descat: LC-MS/MS quantification of the compound.
Sabiha Eddarkaoui: Design and performance of the biological assays.
Caroline Evrard: Cell assays.
Amaury Farce: Molecular modeling.
Marion Gay: Compounds synthesis.
Malika Hamdane: Cellular model.
Mostafa Kouach: LC-MS/MS quantification of the compound.
Paul-Emmanuel Larchanché: Compounds synthesis.
Cyril Laurent: Biochemical analyses of animal models.
Nicolas Lefur: Compounds design and synthesis.
Patricia Melnyk: Co-design the study and writing of the manuscript.
Hélène Obriot: Biochemical analyses of animal models.
Nicolas Sergeant: Co-design of the study and writing of the manuscript.
Valérie Vingtdeux: Development of the cell assay and co-writing of the manuscript.

Acknowledgments

This work was supported by the Inserm, Lille 2 University and CNRS. Grants were obtained from the FRM Nord Pas-de-Calais (France), ANR, Laboratory of Excellence Labex DISTALZ and France Alzheimer. The 300 MHz NMR facilities were funded by the Région Nord Pas-de-Calais (France), the Ministère de la Jeunesse, de l'Education Nationale et de la Recherche (MJENR) and the Fonds Européens de Développement Régional (FEDER). Valérie Vingtdeux is the recipient of a Fondation Plan Alzheimer fellowship. Marion Gay and Caroline Evrard are the recipients of fellowships from Lille 2 University. The authors thank Dr. Paolo Giacobini for proof-reading.

Appendix A. Supplementary data

Supplementary data to this article can be found online at https://doi.org/10.1016/j.nbd.2019.03.028.

References

Acx, H., Chávez-Gutiérrez, L., Serneels, L., Lismont, S., Benurwar, M., Elad, N., De Strooper, B., 2014. Signature β amyloid profiles are produced by different γ-secretase complexes. J. Biol. Chem. 289, 4346–4355.
Barrier, M., Buée, L., Burlet, S., Delacourte, A., Estrella, C., Melnyk, P., Sergeant, N., Verwaerde, P., 2012. Sulfate Salts of *N*-(3-(4-(3-(diisobutylamino)propyl)piperazin-1-yl)propyl)-1*H*-benzo[d]imidazol-2-amine, Preparation Thereof and Use of the Same. (EP 12 306690.4. WO2014/102339).
Barsuto-Islas, G., Grundke-Iqbal, I., Tung, Y.C., Iqbal, K., 2013. Activation of asparaginyl endopeptidase leads to Tau hyperphosphorylation in Alzheimer disease. J. Biol. Chem. 288, 17495–17507.
Belarbi, K., Schindowski, K., Burnouf, S., Caillierez, R., Grosjean, M.E., Demeyer, D., Hamdane, M., Sergeant, N., Blum, D., Buée, L., 2009. Early Tau pathology involving the septo-hippocampal pathway in a Tau transgenic model: relevance to Alzheimer's disease. Curr. Alzheimer Res. 6, 152–157.
Belarbi, K., Burnouf, S., Fernandez-Gomez, F.J., Laurent, C., Lestavel, S., Figeac, M., Sultan, A., Troquier, L., Leboucher, A., Caillierez, R., Grosjean, M.E., Demeyer, D., Obriot, H., Brion, I., Barbot, B., Galas, M.C., Staels, B., Humez, S., Sergeant, N., Schraen-Maschke, S., Muhr-Tailleux, A., Hamdane, M., Buée, L., Blum, D., 2011. Beneficial effects of exercise in a transgenic mouse model of Alzheimer's disease-like Tau pathology. Neurobiol. Dis. 43, 486–494.
Bretteville, A., Ando, K., Ghestem, A., Loyens, A., Bégard, S., Beauvillain, J.C., Sergeant, N., Hamdane, M., Buée, L., 1999. Two-dimensional electrophoresis of tau mutants reveals specific phosphorylation pattern likely linked to early tau conformational changes. PLoS One(4), e4843.
Capurro, V., Busquet, P., Lopes, J.P., Bertorelli, R., Tarozzo, G., Bolognesi, M.L., Piomelli, D., Reggiani, A., Cavalli, A., 2013. Pharmacological characterization of memoquin, a multi-target compound for the treatment of Alzheimer's disease. PLoS One 8 (2), e56870.
Chen, Y., Sun, J., Peng, S., Liao, H., Zhang, Y., Lehmann, J., 2013. Tacrine-flurbiprofen hybrids as multifunctional drug candidates for the treatment of Alzheimer's disease. Arch. Pharm. 346, 865–871.
Cummings, J., Lee, G., Mortsdorf, T., Ritter, A., Zhong, K., 2017. Alzheimer's disease drug development pipeline: 2017. Alzheimer's Dement Transl. Res. Clin. Interv. 3, 367–384.
De Strooper, B., 2010. Proteases and proteolysis in Alzheimer disease: a multifactorial view on the disease process. Physiol. Rev. 90, 465–494.
Domise, M., Didier, S., Marinangeli, C., Zhao, H., Chandakkar, P., Buée, L., Viollet, B., Davies, P., Marambaud, P., Vingtdeux, V., 2016. AMP-activated protein kinase modulates tau phosphorylation and tau pathology in vivo. Sci. Rep. 6, 26758.
Dubois, B., Feldman, H.H., Jacova, C., Cummings, J.L., Dekosky, S.T., Barberger-Gateau, P., Delacourte, A., Frisoni, G., Fox, N.C., Galasko, D., Gauthier, S., Hampel, H., Jicha, G.A., Meguro, K., O'Brien, J., Pasquier, F., Robert, P., Rossor, M., Salloway, S., Sarazin, M., de Souza, L.C., Stern, Y., Visser, P.J., Scheltens, P., 2010. Revising the definition of Alzheimer's disease: a new lexicon. Lancet Neurol. 9, 1118–1127.
Ellman, G.L., Courtney, K.D., Andres Jr., V., Featherstone, R.M., 1961. A new and rapid colorimetric determination of acetylcholinesterase activity. Biochem. Pharmacol. 7, 88–90.
Fernandez-Gomez, F.J., Jumeau, F., Derisbourg, M., Burnouf, S., Tran, H., Eddarkaoui, S., Obriot, H., Dutoit-Lefevre, V., Deramecourt, V., Mitchell, V., Lefranc, D., Hamdane, M., Blum, D., Buée, L., Buée-Scherrer, V., Sergeant, N., 2014. Consensus brain-derived protein, extraction protocol for the study of human and murine brain proteome using both 2D-DIGE and mini 2DE immunoblotting. J. Vis. Exp.(86).
Hu, M.K., 2001. Synthesis and in-vitro anticancer evaluation of bistacrine congeners. J. Pharm. Pharmacol. 53, 83–88.
Inoue, K., Rispoli, J., Kaphzan, H., Klann, E., Chen, E.I., Kim, J., Komatsu, M., Abeliovich, A., 2012. Macroautophagy deficiency mediates age-dependent neurodegeneration through a phospho-tau pathway. Mol. Neurodegener. 7, 48–60.

Ittner, L.M., Ke, Y.D., Delerue, F., Bi, M., Gladbach, A., van Eersel, J., Wölfing, H., Chieng, B.C., Christie, M.J., Napier, I.A., Eckert, A., Staufenbiel, M., Hardeman, E., Götz, J., 2010. Dendritic function of tau mediates amyloid-beta toxicity in Alzheimer's disease mouse models. Cell 142, 387–397.

Van der Jeugd, A., Ahmed, T., Burnouf, S., Belarbi, K., Hamdame, M., Grosjean, M.E., Humez, S., Balschun, D., Blum, D., Buée, L., D'Hooge, R., 2011. Hippocampal tauopathy in tau transgenic mice coincides with impaired hippocampus-dependent learning and memory, and attenuated late-phase long-term depression of synaptic transmission. Neurobiol. Learn. Mem. 95 (3), 296–304.

Jiang, P., Mizushima, N., 2015. LC3- and p62-based biochemical methods for the analysis of autophagy progression in mammalian cells. Methods 75, 13–18.

Keri, R.S., Quintanova, C., Marques, S.M., Esteves, A.R., Cardoso, S.M., Santos, M.A., 2013. Design, synthesis and neuroprotective evaluation of novel tacrine–benzothiazole hybrids as multi-targeted compounds against Alzheimer's disease. Bioorg. Med. Chem. 21, 4559–4569.

Laurent, C., Burnouf, S., Ferry, B., Batalha, V.L., Coelho, J.E., Baqi, Y., Malik, E., Marciniak, E., Parrot, S., Van der Jeugd, A., Faivre, E., Flaten, V., Ledent, C., D'Hooge, R., Sergeant, N., Hamdane, M., Humez, S., Müller, C.E., Lopes, L.V., Buée, L., Blum, D., 2016. A_{2A} adenosine receptor deletion is protective in a mouse model of Tauopathy. Mol. Psychiatry 21 (1), 97–107.

Le Freche, H., Brouillette, J., Fernandez-Gomez, F.J., Patin, P., Caillierez, R., Zommer, N., Sergeant, N., Buée-Scherrer, V., Lebuffe, G., Blum, D., Buée, L., 2012. Tau phosphorylation and sevoflurane anesthesia: an association to postoperative cognitive impairment. Anesthesiology 116, 779–787.

Mangialasche, F., Solomon, A., Winblad, B., Mecocci, P., Kivipelto, M., 2010. Alzheimer's disease: clinical trials and drug development. Lancet Neurol. 9, 702–716.

Melnyk, P., Sergeant, N., Buée, L., Delacourte, A., 2006. Use of 1,4-bis(3-aminopropyl) Piperazine Derivatives in Therapy. (WO 2006 051489).

Melnyk, P., Vingtdeux, V., Burlet, S., Eddarkaoui, S., Grosjean, M.E., Larchanché, P.E., Hochart, G., Sergheraert, C., Estrella, C., Barrier, M., Poix, V., Plancq, P., Lannoo, C., Hamdane, M., Delacourte, A., Verwaerde, P., Buée, L., Sergeant, N., 2015. Chloroquine and chloroquine related compounds as a model for the design of anti-Alzheimer compounds. ACS Chem. Neurosci. 6, 559–569.

Munoz-Torrero, D., 2008. Acetylcholinesterase inhibitors as disease-modifying therapies for Alzheimer's disease. Curr. Med. Chem. 15, 2433–2455.

Nijholt, D.A.T., Nölle, A., van Haastert, E.S., Edelijn, H., Toonen, R.F., Hoozemans, J.J.M., Scheper, W., 2013. Unfolded protein response activates glycogen synthase kinase-3 via selective lysosomal degradation. Neurobiol. Aging 34, 1759–1771.

Nixon, R.A., 2013. The role of autophagy in neurodegenerative diseases. Nat. Med. 19, 983–997.

Pardossi-Piquard, R., Checler, F., 2012. The physiology of the β-amyloid precursor protein intracellular domain AICD. J. Neurochem. 120 (Suppl. 1), 109–124.

Pickford, F., Masliah, E., Britschgi, M., Lucin, K., Narasimhan, R., Jaeger, P.A., Small, S., Spencer, B., Rockenstein, E., Levine, B., Wyss-Coray, T., 2008. The autophagy-related protein beclin1 shows reduced expression in early Alzheimer disease and regulates amyloid beta accumulation in mice. J. Clin. Invest. 118, 2190–2199.

Polito, V.A., Li, H., Martini-Stoica, H., Wang, B., Yang, L., Xu, Y., Swartzlander, D.B., Palmieri, M., di Ronza, A., Lee, V.M., Sardiello, M., Ballabio, A., Zheng, H., 2014. Selective clearance of aberrant tau proteins and rescue of neurotoxicity by transcription factor EB. EMBO Mol. Med. 6, 1142–1160.

Pooler, A.M., Polydoro, M., Maury, E.A., 2015. Amyloid accelerates tau propagation and toxicity in a model of early Alzheimer's disease. Acta Neuropathol. 129, 895–907.

Ryckebusch, A., Deprez-Poulain, R., Maes, L., Debreu-Fontaine, M.-A., Mouray, E., Grellier, P., Sergheraert, C., 2003. Synthesis and in vitro and in vivo antimalarial activity of N1-(7-Chloro-4-quinolyl)-1,4-bis(3-aminopropyl)piperazine derivatives. J. Med. Chem. 46, 542–557.

Sergeant, N., David, J.P., Goedert, M., Jakes, R., Vermersch, P., Buée, L., Lefranc, D., Wattez, A., Delacourte, A., 1997. Two-dimensional characterization of paired helical filament-tau from Alzheimer's disease: demonstration of an additional 74-kDa component and age-related biochemical modifications. J. Neurochem. 69 (2), 834–844.

Sergeant, N., Wattez, A., Delacourte, A., 1999. Neurofibrillary degeneration in progressive supranuclear palsy and corticobasal degeneration: tau pathologies with exclusively « exon 10 » isoforms. J. Neurochem. 72, 1243–1249.

Sergeant, N., David, J.P., Champain, D., Ghestem, A., Wattez, A., Delacourte, A., 2002. Progressive decrease of amyloid precursor protein carboxy terminal fragments (APP-CTFs), associated with tau pathology stages, in Alzheimer's disease. J. Neurochem. 81, 663–672.

Spencer, B., Potkar, R., Trejo, M., Rockenstein, E., Patrick, C., Gindi, R., Adame, A., Wyss-Coray, T., Masliah, E., 2009. Beclin 1 gene transfer activates autophagy and ameliorates the neurodegenerative pathology in alpha-synuclein models of Parkinson's and Lewy body diseases. J. Neurosci. 29, 13578–13588.

Takahashi, M., Miyata, H., Kametani, F., Nonaka, T., Akiyama, H., Hisanaga, S., Hasegawa, M., 2015. Extracellular association of APP and tau fibrils induces intracellular aggregate formation of tau. Acta Neuropathol. 129, 895–907.

Tam, J.H., Seah, C., Pasternak, S.H., 2014. The Amyloid Precursor Protein is rapidly transported from the Golgi apparatus to the lysosome and where it is processed into beta-amyloid. Mol. Brain 7, 54–71.

Troquier, L., Caillierez, R., Burnouf, S., Fernandez-Gomez, F.J., Grosjean, M.E., Zommer, N., Sergeant, N., Schraen-Maschke, S., Blum, D., Buée, L., 2012. Targeting phospho-Ser422 by active Tau immunotherapy in the THYTau22 mouse model: a suitable therapeutic approach. Curr. Alzheimer Res. 9, 397–405.

Vingtdeux, V., Marambaud, P., 2012. Identification and biology of α-secretase. J. Neurochem. 120 (Suppl. 1), 34–45.

Vingtdeux, V., Hamdane, M., Loyens, A., Gelé, P., Drobecq, H., Bégard, S., Galas, M.C., Delacourte, A., Beauvillain, J.C., Buée, L., Sergeant, N., 2007. Alkalizing drugs induce accumulation of amyloid precursor protein by-products in luminal vesicles of multivesicular bodies. J. Biol. Chem. 282, 18197–18205.

Vorobyeva, A.G., Lee, R., Miller, S., Longen, C., Sharoni, M., Kandelwal, P.J., Kim, F.J., Marenda, D.R., Saunders, A.J., 2014. Cyclopamine modulates γ-secretase-mediated cleavage of amyloid precursor protein by altering its subcellular trafficking and lysosomal degradation. J. Biol. Chem. 289, 33258–33274.

Ye, X., Cai, Q., 2014. Snapin-mediated BACE1 retrograde transport is essential for its degradation in lysosomes and regulation of APP processing in neurons. Cell Rep. 6, 24–31.

Zhang, Z., Song, M., Liu, X., Kang, S.S., Kwon, I.S., Duong, D.M., Seyfried, N.T., Hu, W.T., Liu, Z., Wang, J.Z., Cheng, L., Sun, Y.E., Yu, S.P., Levey, A.I., Ye, K., 2014. Cleavage of tau by asparagine endopeptidase mediates the neurofibrillary pathology in Alzheimer's disease. Nat. Med. 20, 1254–1262.